

Interpretability-by-Design with Accurate Locally Additive Models and Conditional Feature Effects

Vasilis Gkolemis^{1,2} Loukas Kavouras¹ Dimitrios Kyriakopoulos¹ Konstantinos Tsopelas¹
 Dimitrios Rontogiannis³ Giuseppe Casalicchio⁴ Theodore Dalamagas¹ Christos Diou²

Abstract

Generalized additive models (GAMs) offer interpretability through independent univariate feature effects but underfit when interactions are present in data. GA²Ms add selected pairwise interactions which improves accuracy, but sacrifices interpretability and limits model auditing. We propose *Conditionally Additive Local Models* (CALMs), a new model class, that balances the interpretability of GAMs with the accuracy of GA²Ms. CALMs allow multiple univariate shape functions per feature, each active in different regions of the input space. These regions are defined independently for each feature as simple logical conditions (thresholds) on the features it interacts with. As a result, effects remain locally additive while varying across subregions to capture interactions. We further propose a principled distillation-based training pipeline that identifies homogeneous regions with limited interactions and fits interpretable shape functions via region-aware backfitting. Experiments on diverse classification and regression tasks show that CALMs consistently outperform GAMs and achieve accuracy comparable with GA²Ms. Overall, CALMs offer a compelling trade-off between predictive accuracy and interpretability.

1. Introduction

In high-stakes decision making, machine learning models must provide not only reliable predictions but also human-understandable explanations (Murdoch et al., 2019; Doshi-Velez & Kim, 2017). This requirement has motivated the development of *interpretable-by-design* models, whose structure permits direct inspection of their behavior (Molnar, 2020). However, interpretability is a continuum rather than

¹ATHENA RC, Greece ²HUA, Greece ³Max Planck ISS, Germany ⁴LMU, Germany. Correspondence to: Vasilis Gkolemis <vgkolemis@athenarc.gr>.

a binary property: interpretable-by-design models span a spectrum where gains in predictive accuracy often entail greater structural complexity (Rudin, 2019; Lipton, 2018).

This trade-off is particularly evident in GAMs (Lou et al., 2012) and, their extension, GA²M (Caruana et al., 2015). GAMs achieve high interpretability by modeling predictions as a sum of independent univariate effects, but this strict additivity prevents them from capturing feature interactions, limiting their predictive accuracy. GA²Ms add selected pairwise interactions, improving performance at the cost of crucial interpretability properties (Radenovic et al., 2022). Specifically, interaction terms (i) obscure the unique attribution of the prediction to individual features because the pairwise interaction terms are generally not additively separable (ii) complicate global auditing by requiring the simultaneous inspection of multiple (univariate and bivariate) effects. Section 3.3 analyzes these limitations in detail.

We introduce *Conditionally Additive Local Models* (CALMs), a new model class that strikes a balance between the predictive accuracy of GA²Ms and the interpretability of GAMs. The core idea is to learn *conditional feature effects*: multiple univariate effects per feature, each active within a distinct region of the input space where the feature exhibits nearly additive behavior—that is, where it minimally interacts with others. These regions are defined through threshold-based conditions on interacting features. For example, if x_i interacts with x_j , a CALM may learn separate effects for x_i ; one when $x_j < \tau$ and another when $x_j \geq \tau$ for some threshold τ . Figure 1 illustrates this representation. Conditional effects thus enable interaction-aware modeling while maintaining (i) transparent feature contributions and (ii) straightforward global model auditing.

To fit CALMs to data, we propose a three-step distillation-based pipeline: (1) Train a black-box reference model to capture complex interactions present in the data; (2) Partition the input space independently for each feature using CART-based splitters (Herbinger et al., 2022) optimized to minimize heterogeneity—a criterion that, when minimized, provably reduces feature interactions within the resulting regions (Herbinger et al., 2024); (3) Fit region-specific shape functions using a region-aware extension

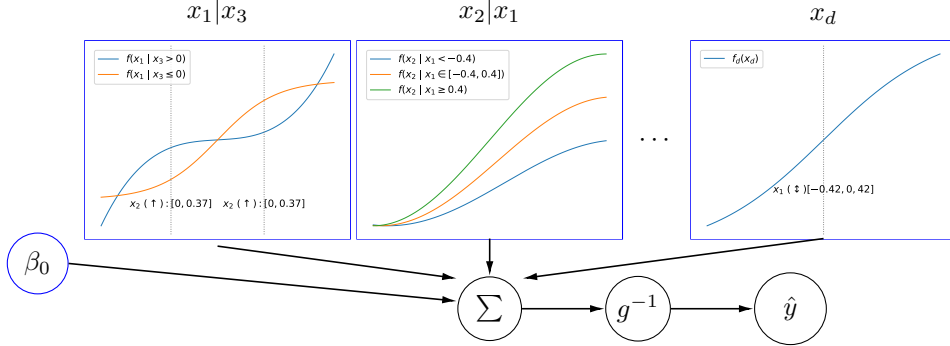


Figure 1. CALMs use *conditional feature effects*: every feature effect is expressed by a collection of 1D functions, each associated with a different region of the input space. In the example, the effect of x_1 conditions on x_3 , the effect of x_2 on x_1 , while x_d does not interact with any other feature and thus has a single plot. CALMs are *interpretable-by-design*—summarized in d figures of 1D plots—and *accurate*, as they can model feature interactions. **Code available at:** <https://github.com/givasile/CALM>.

of the standard backfitting algorithm. This procedure efficiently identifies interacting features (e.g., x_i interacts with x_j), optimal split points (e.g., τ such that separate effects are learned for $x_j < \tau$ and $x_j \geq \tau$), and requires minimal tuning—primarily the maximum allowed number of interactions per feature.

Extensive evaluation on diverse regression and classification benchmarks demonstrates that CALMs consistently outperform GAMs in predictive accuracy, and often match or exceed GA²Ms. Furthermore, we formally show that CALMs satisfy key interpretability properties unsupported by GA²Ms. Code for reproducing all experiments is provided in the supplementary material.

Contributions. (i) We introduce *Conditionally Additive Local Models* (CALMs), a novel interpretable-by-design model class that balances GAM’s interpretability and GA²Ms accuracy via conditional feature effects. (ii) We develop a robust training algorithm based on distillation, heterogeneity-minimization and region-aware backfitting. (iii) We provide a formal analysis of the interpretability properties inherent in CALMs. (iv) We present extensive empirical evidence demonstrating improved accuracy–interpretability trade-offs over GAMs and GA²Ms.

2. Background and Related Work

Interpretable-by-design models enforce transparency in their decision-making process. Examples include decision trees (Breiman et al., 1984), rule lists (Letham et al., 2015; Angelino et al., 2018), and prototype-based classifiers (Chen et al., 2019; Bien & Tibshirani, 2011). Among them, GAMs (Hastie & Tibshirani, 1990; Wood, 2017) stand as a particularly popular candidate, mainly due to their simple global interpretability.

GAMs model the output as $g(\mathbb{E}[y]) = \beta_0 + \sum_i f_i(x_i)$, where each f_i is a univariate shape function, β_0 is the

global intercept, and g is a link function. The key benefit of GAMs is that feature effects can be *independently* visualized through a simple 1D plot. Methods for learning $f_i \forall i$ include spline-based approaches (Lou et al., 2012; Wood, 2017), gradient boosting (Friedman, 2001), and neural-based variants (Agarwal et al., 2021; Kraus et al., 2024; Radenovic et al., 2022). However, standard GAMs assume that features contribute independently to the output, which limits their accuracy when feature interactions are present in data.

To capture these interactions, GA²Ms add pairwise terms: $g(\mathbb{E}[y]) = \beta_0 + \sum_i f_i(x_i) + \sum_{i < j} f_{ij}(x_i, x_j)$ (Lou et al., 2013). GA²Ms instances vary in (i) how they select the top- K interactions to maintain sparsity and (ii) how they learn f_i and f_{ij} . For example, (Lou et al., 2013) greedily selects interactions based on loss reduction, while, neural-based approaches (Yang et al., 2020; Ibrahim et al., 2023; Chang et al., 2022) integrate pairwise interactions into standard neural-based architectures.

While GA²Ms improve accuracy, they obscure individual feature contributions and complicate model auditing (see Section 3.3). A key open question remains: *Can we achieve GA²M-level accuracy while maintaining GAM-level interpretability?* To this end, we draw inspiration from *regional effect methods*, which handle interactions by partitioning the feature space into subregions where interactions are weak.

To understand regional effects, consider first how standard global effect work. Global effect plots, such as PDP, ALE or SHAP-DP, explain a black box model by decomposing its complex d -dimensional function $f(\mathbf{x}) \rightarrow y$ into d one-dimensional plots $x_i \rightarrow y$. However, when strong interactions exist between x_i and other features, these plots can yield misleading explanations (Gkolemis et al., 2023a;b).

Regional feature effect plots address that by partitioning the feature space into subregions where interactions are minimal (Herbinger et al., 2022; 2024). Within each subregion,

simple univariate plots accurately represent feature effects without being confounded by interactions with other features. We adopt this strategy to identify low-interaction subregions and then we fit shape functions within each subregion.

Our approach relates to model distillation (Hinton et al., 2015; Tan et al., 2018) and surrogate modeling (Guidotti et al., 2018). These approaches train an interpretable “student” model to mimic a complex “teacher”, either locally (Ribeiro et al., 2016) or globally (Guidotti et al., 2018). However, instead of explaining the teacher, we use it to identify subregions with minimal feature interactions, on which we then fit shape functions. In a rough analogy, CALM serves as the interpretable-by-design “student” that replaces the black-box “teacher” as the final predictor.

Other works that share the above idea are: SLIM (Hu et al., 2020) and related analyses (Herbinger et al., 2023) propose tree-based models with simple predictors in each region, mainly in the context of model distillation and explanation. In contrast, our goal is not to approximate a black-box model, but to construct an interpretable-by-design predictor with GAM-like structure. Related ideas also appear in (Gkolemis et al., 2023c), which leverages regional feature effects to build interpretable models; however, that work does not explicitly characterize the interpretability guarantees of the learned model or evaluate them systematically.

3. CALM: Conditionally Additive Local Model

CALM captures feature interactions via *conditional feature effects*, a set of univariate shape functions per feature, each active in a different region of the input space.

3.1. Model Formulation

Let $\mathbf{X} = (X_1, \dots, X_d) \in \mathcal{X} \subseteq \mathbb{R}^d$ be a random vector with joint distribution $P_{\mathbf{X}}$ over the input data, $\mathbf{x} = (x_1, \dots, x_d)$ where $\mathcal{X} = \mathcal{X}_1 \times \dots \times \mathcal{X}_d$. We use the subscript $-i$ to denote quantities excluding the i -th feature (e.g., \mathbf{X}_{-i} defined on space \mathcal{X}_{-i}). Let also Y be the output random variable, with $Y \in \mathbb{R}$ for regression and $Y \in \{0, 1\}$ for binary classification. CALM is then defined as

$$g(\mathbb{E}[Y | \mathbf{X} = \mathbf{x}]) = \beta_0 + \sum_{i=1}^d f_i^{(r_i(\mathbf{x}_{-i}))}(x_i) \quad (1)$$

where $\beta_0 \in \mathbb{R}$ is an intercept and g is a link function (identity for regression and logit for classification). For each feature i , CALM learns a set of univariate shape functions $\{f_i^{(r)}\}_{r=1}^{R_i}$. At prediction time, a region selection function $r_i(\mathbf{x}_{-i}) : \mathbb{R}^{d-1} \rightarrow \{1, \dots, R_i\}$ chooses the specific shape function for x_i based on the context of other features \mathbf{x}_{-i} . This allows the effect of x_i to vary across regions, effectively modeling feature interactions, while maintaining univariate

interpretability within each region. The final prediction is given by:

$$f_{\text{CALM}}(\mathbf{x}) = g^{-1} \left(\beta_0 + \sum_{i=1}^d f_i^{(r_i(\mathbf{x}_{-i}))}(x_i) \right) \quad (2)$$

For the rest of the paper, we may use $\hat{y}(\mathbf{x})$ to denote f_{CALM} for brevity. The selection function $r_i(\mathbf{x}_{-i})$ partitions the input space (excluding x_i) into $\mathcal{P}_i := \{\mathcal{R}_i^{(r)}\}_{r=1}^{R_i}$, independently for each feature i , where each $\mathcal{R}_i^{(r)} \subseteq \mathcal{X}_{-i}$. The goal of these partitions is to minimize interactions between x_i and other features within each region, ensuring the effect of x_i is accurately captured by a single univariate shape function. To maintain interpretability, each partition is represented by a binary decision tree T_i of maximum depth d_{max} , built over \mathbf{x}_{-i} . Internal nodes apply axis-aligned splits, i.e., inequality thresholds $x_j < \tau$ or $x_j \geq \tau$ for continuous features, and equality tests $x_j = \tau$ or $x_j \neq \tau$ for categorical ones. Each leaf of the tree defines a region $\mathcal{R}_i^{(r)}$. Formally, each region is defined by a conjunction of at most $m_i^{(r)} \leq d_{max}$ rules:

$$\mathcal{R}_i^{(r)} = \left\{ \mathbf{x}_{-i} \mid \wedge_{k=1}^{m_i^{(r)}} (x_{j_k} \text{ op}_k \tau_k) \right\}. \quad (3)$$

where $j_k \in \{1, \dots, d\} \setminus \{i\}$ indexes an interacting feature, $\text{op}_k \in \{<, \geq, =, \neq\}$ is a comparison operator, and $\tau_k \in \mathbb{R}$ is a threshold.

CALM is able to capture feature interactions involving up to $(d_{max}+1)$ features, as each region conditions on up to d_{max} features. While increasing d_{max} can improve accuracy, it comes at the cost of interpretability.

To balance this accuracy-interpretability tradeoff, CALM exposes two hyperparameters: d_{max} (tree depth) bounds the number of shape functions per feature to $R_i \leq 2^{d_{max}}$, while K limits the total number of shape functions across all features via $\sum_i R_i \leq K$. In our experiments, we set $d_{max} = 2$ (yielding $R_i = 4$ regions per feature) and leave K unconstrained.

Notably, CALM learns, at most, $d \cdot 2^{d_{max}}$ univariate shape functions (up to $2^{d_{max}}$ per feature), yet these combine to express up to $2^{d \cdot d_{max}}$ distinct additive models—an exponential increase in expressive power.

3.2. Training algorithm for fitting CALM

Given a dataset $\mathcal{D} = \{(\mathbf{x}^{(i)}, y^{(i)})\}_{i=1}^N$, we fit a CALM predictor by minimizing the empirical risk $\mathbb{E}_{(\mathbf{X}, Y) \sim \hat{P}_{\mathcal{D}}} [\mathcal{L}(Y, \hat{y}(\mathbf{X}))]$, where $\hat{y}(\mathbf{X})$ denotes a CALM model, \mathcal{L} a loss function and $\hat{P}_{\mathcal{D}}$ the empirical distribution over \mathcal{D} . Fitting a CALM requires estimating: (a) a set of d partitions \mathcal{P}_i , $i \in \{1, \dots, d\}$, represented by binary trees T_i (one per feature); (b) region-specific shape functions

Algorithm 1 Training a CALM model

Require: Training data $\mathcal{D} = \{(\mathbf{x}^{(i)}, y^{(i)})\}_{i=1}^N$
Output: CALM predictor $f_{\text{CALM}}(\mathbf{x})$

- 1: **Step 1:** Train reference model f_{ref} on \mathcal{D} .
- 2: **Step 2:** Learn feature-specific trees $T_i, i = 1, \dots, d$.
- 3: **Step 3:** Estimate shape functions $\{\{f_i^{(r)}\}_{r=1}^{R_i}\}_{i=1}^d$.

$\{f_i^{(r)}\}_{r=1}^{R_i}$ and a global intercept β_0 . We propose a three-step distillation-based pipeline summarized in Algorithm 1.

Step 1: Train a Reference Model. We train a high-capacity black-box predictor $f_{\text{ref}} : \mathcal{X} \rightarrow \mathbb{R}$ on \mathcal{D} . This model serves as functional proxy for $\mathbb{E}[Y|\mathbf{X}]$ and is used exclusively to detect interactions. The reference model is discarded after training. The choice of f_{ref} is independent of later stages; any accurate predictor can be used, such as gradient-boosted trees (our default), neural networks, random forests or foundation models, like TabPFN (Hollmann et al., 2022).

Step 2: Learn feature-specific partitioning trees.

This step learns d independent, feature-specific partitions $\mathcal{P}_i := \{\mathcal{R}_i^{(r)}\}_{r=1}^{R_i}$, each represented by a binary tree T_i defined over \mathbf{x}_{-i} . The objective is to identify near-additive regions $\mathcal{R}_i^{(r)}$, in which the effect of x_i on the output is well approximated by a univariate function $f_i^{(r)}$, due to locally weak higher-order interactions.

To identify such regions, we use the interaction-related heterogeneity measure from (Herbinger et al., 2024). Feature effect methods (e.g., PDP or ALE) explain a black-box model (like $f_{\text{ref}}(\mathbf{x})$) by decomposing it into univariate effects $f_i(x_i) \forall i$. To do so, they first define the local effects $h(x_i, \mathbf{x}_{-i}^{(j)})$ that quantify the contribution of feature x_i on a specific instance $\mathbf{x}^{(j)}$. Then they compute $f_i(x_i)$ by averaging the local effects. Heterogeneity is the variability of these local effects around their average, directly measuring how much x_i 's effect depends on other features. High heterogeneity signals strong interactions, while low heterogeneity identifies near-additive, interaction-free regions—making it an effective criterion for our purpose.

Following the above, we define the *pointwise* heterogeneity of x_i in a region \mathcal{R} (e.g., $\mathcal{R}_i^{(r)}$) as:

$$H_i^{\mathcal{R}}(x_i) = \mathbb{E}_{\mathbf{X}_{-i}|\mathbf{X}_{-i} \in \mathcal{R}} \left[(h(x_i, \mathbf{X}_{-i}) - \mu_i^{\mathcal{R}}(x_i))^2 \right] \quad (4)$$

where $\mu_i^{\mathcal{R}}(x_i) = \mathbb{E}_{\mathbf{X}_{-i}|\mathbf{X}_{-i} \in \mathcal{R}} [h(x_i, \mathbf{X}_{-i})]$

The corresponding *feature-level heterogeneity* is:

$$H_i^{\mathcal{R}} = \mathbb{E}_{X_i|\mathbf{X}_{-i} \in \mathcal{R}} [H_i^{\mathcal{R}}(X_i)] \quad (5)$$

In our experiments, heterogeneity is computed using PDP-based formulas. As shown in (Herbinger et al., 2024), ALE- and SHAP-DP variants also provide valid alternatives; we refer to (Herbinger et al., 2022; 2024) for details.

As additional theoretical justification for using heterogeneity as the splitting criterion, we show that, under specific assumptions, the approximation error of CALM is bounded by the sum of the expected feature heterogeneities. Consequently, reducing heterogeneity of each feature through partitioning yields a CALM model f_{CALM} with lower mean squared error, assuming perfect fit in Step 3 of Algorithm 1. The proof is provided in Appendix A (Proposition A.1).

Therefore, we use $H_i^{\mathcal{R}}$ as the splitting criterion and learn a binary decision tree T_i for each feature x_i using a greedy CART-style algorithm. At each node, we consider splits over all conditioning features $x_j \neq x_i$ and select the split that maximizes the reduction in heterogeneity. For numerical features, splits take the form $x_j \{\leq, >\} \tau$, while for categorical features we use $x_j \{=, \neq\} \tau$. A split is accepted only if the relative reduction in $H_i^{\mathcal{R}}$ exceeds a threshold ϵ ; otherwise, the node becomes a leaf. This procedure yields a partition $\mathcal{P}_i = \{\mathcal{R}_i^{(r)}\}_{r=1}^{R_i}$ where heterogeneity is significantly reduced, ensuring the effect of x_i is locally stable and less distorted by interactions than in the global space. Additional implementation details are provided in Appendix A. In all experiments, we use PDP-based heterogeneity, set the maximum tree depth to $d_{\max} = 2$, and fix $\epsilon = 0.2$.

Step 3: Estimate Shape Functions. Given the partitions $\{\mathcal{P}_i\}_{i=1}^d$, we estimate the region-specific shape functions $\{f_i^{(r)}\}$ by minimizing the empirical loss of the CALM predictor. We use a modified gradient boosting procedure in which, at each iteration, a single shape function $f_i^{(r)}$ is updated using only the observations whose \mathbf{x}_{-i} fall into the corresponding region $\mathcal{R}_i^{(r)}$ (see Appendix A for details).

Although each update is restricted to a single region, the resulting optimization problem is inherently *coupled*. The regions are defined separately for each feature, so the subsets of samples used to update different shape functions generally overlap. Consequently, updating one $f_i^{(r)}$ changes the residuals seen by all other shape functions. Therefore it can be understood as a coordinated optimization of a single additive predictor with region-gated components.

The following proposition formalizes this intuition by characterizing the target of Step 3 at the population level and its convergence behavior under idealized updates. The proof is in Appendix A. In practice, Step 3 is implemented using gradient boosting to approximate the exact regional updates.

Proposition 3.1 (Optimality and convergence). *Let $m(\mathbf{x}) = \mathbb{E}[Y | \mathbf{X} = \mathbf{x}]$ denote the true regression function. Assume regression with squared loss, fixed partition trees $\{T_i\}_{i=1}^d$ (as learned by Step 2) and $\mathbb{E}[Y^2] < \infty$. Let $\mathcal{H}(\{T_i\})$ denote the fixed-tree CALM class (Appendix A.3.1), and assume $\mathcal{H}(\{T_i\}) \subset L_2(P_X)$ is nonempty, closed, and convex. Then:*

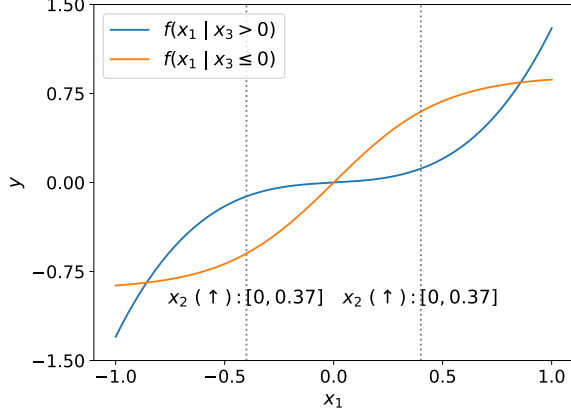


Figure 2. CALM plot for x_1 . Each curve shows the contribution of x_1 to y (P1) in a different region of the input space ($x_3 \leq 0$). Vertical lines indicate interaction-induced discontinuities, e.g., at $x_1 \approx -0.4$ there exist a positive hidden jump of $[0, 0.37]$ due to interaction of x_1 with x_2 , which must be considered when assessing regional sensitivity (P2) or global properties (P3).

1. Optimality: Any $s^* \in \arg \min_{s \in \mathcal{H}(\{T_i\})} \mathbb{E}[(Y - s(\mathbf{X}))^2]$ is the $L_2(P_{\mathbf{X}})$ -best approximation of m within $\mathcal{H}(\{T_i\})$.
2. Convergence: The idealized exact cyclic regional back-fitting converges to an empirical risk minimizer over $\mathcal{H}(\{T_i\})$.

3.3. Interpretability of a CALM

CALMs offer interpretability similar to GAMs, as both require inspecting d univariate plots; one per feature. CALMs are slightly more complex: unlike GAMs, each plot can contain up to $2^{d_{\max}}$ curves corresponding to a different region of the input space and with interaction-induced discontinuities marked by vertical lines. However, because regions are interpretable (specified by simple threshold conditions), these region-specific curves provide explanations which are suitable for model auditing and decision support. For example: *The effect of age on mortality rate follows this curve when the patient is male and has a BMI above 30.*

Interpreting a CALM plot. In Figure 2 each curve gives the contribution of x_1 to y in a specific region; the blue curve when $x_3 > 0$ and the orange curve when $x_3 \leq 0$. For example, at $x_1 = -0.5$, the contribution is approximately -0.2 (blue) or -0.75 (orange), depending on x_3 . The plots also illustrate how altering x_1 to $x_1 \rightarrow x_1 + \Delta x$ impacts the prediction. Vertical dotted lines mark points of a hidden discontinuity which is due to x_1 participating as an interaction term for feature x_2 . As shown in Figure 1, the effect of x_2 is conditioned by $x_1 \leq -0.4$, $-0.4 \leq x_1 \leq 0.4$ and $x_1 > 0.4$, therefore in Figure 2 we observe vertical lines in $x_1 \pm 0.4$. If a change in x_1 does not cross a vertical line, the change in the output (Δy) equals the curve difference

(Δf_i). Crossing a line signifies a hidden jump, in the range $[\alpha, \beta]$, so $\Delta f_i + \alpha \leq \Delta y \leq \Delta f_i + \beta$. Arrows provide a fast understanding of the jump: \uparrow means $\Delta y > \Delta f_i$, \downarrow means $\Delta y < \Delta f_i$, $\uparrow\downarrow$ means it depends.

Below, we outline three crucial interpretability properties, along with discussion about their satisfiability by GAM, GA²M, and CALM. Complete proofs are provided in Appendix B.

P1. Local Feature Contribution: What is the contribution of each feature to the prediction?

Formally: Given an input \mathbf{x} , how much does each x_i contribute to $\hat{y}(\mathbf{x})$?

The explanation is *local*—it concerns a specific input \mathbf{x} . In GAM, the contribution is $f_i(x_i)$. In GA²M, the contribution is neither explicit nor unique; it must be inferred post-hoc (e.g., via SHAP or LIME), with each method relying on different assumptions and yielding different results. In CALM, the contribution is $f_i^{(r(\mathbf{x}_{-i}))}(x_i)$.

P2. Regional Feature Sensitivity: How does changing x_i change the prediction?

Formally: Given x_i and $\Delta x > 0$, what is $\Delta \hat{y} = \hat{y}(\mathbf{x} + \mathbf{e}_i \Delta x) - \hat{y}(\mathbf{x})$, assuming only x_i is perturbed and \mathbf{x}_{-i} is fixed?

The explanation is *regional*—it characterizes the effect of x_i on a specific region ($[x_i, x_i + \Delta x]$) *independently* of the values of other features. In GAM, the change is $\Delta \hat{y} = f_i(x_i + \Delta x) - f_i(x_i)$. In GA²M, the change cannot be determined without knowing the values of all features that interact with x_i . In CALM, an exact answer is possible only when the perturbation does not cross a vertical line. In this case, the resulting change is a set of values $\Delta y := \{\Delta f_i^{(r)}\}_{r=1}^{R_i}$, one for each curve in the plot: $\Delta f^{(r)} = f_i^{(r)}(x_i + \Delta x) - f_i^{(r)}(x_i)$. If a crossing occurs, an exact answer is not attainable, however, for less precise questions, such as whether the Δx change in x_i will have a positive impact on y , an answer is still feasible (see P3. below).

P3. Global Feature Property: Is the model globally monotonic increasing with respect to x_i ?

Formally: For all \mathbf{x} and $\Delta x > 0$, is $\Delta \hat{y} = \hat{y}(\mathbf{x} + \mathbf{e}_i \Delta x) - \hat{y}(\mathbf{x}) > 0$?

The explanation is *global*—it assesses the monotonicity of x_i across the entire input space. In GAM, monotonicity is easily determined by the shape of $f_i(x_i)$. In GA²M, verifying monotonicity requires a concurrent examination of the 1D shape of $f_i(x_i)$ along with all pairwise interactions f_{ij} along all j , an inspection which is infeasible for a human. In CALM, if no vertical lines are present, simply check whether all curves $f_i^{(r)}(x_i)$ for $r = 1, \dots, R_i$ are monotonically increasing. If vertical lines exist, simply verify that

all arrows are positive.

3.4. Efficiency

The efficiency of fitting a CALM to a dataset is mainly affected by the number of instances N and the feature dimensionality d .

Step 1 involves fitting a black box model, which, in general, is computationally efficient. Our default setup uses an XGBoost model that fits in a few seconds.

Step 2 is the computational bottleneck as it requires fitting d binary trees T_i , resulting in a worst-case cost of $\mathcal{O}(d_{\max} d^2 N \log N)$. Since the trees are shallow (d_{\max} is small), this reduces to $\mathcal{O}(d^2 N \log N)$, which is acceptable in practice given that d is typically on the order of tens for tabular datasets. Crucially, the local effects needed for evaluating candidate splits are computed once for the entire dataset and stored. Then, at each candidate split, the algorithm checks the precomputed effects that relate to the samples in the node (indexed lookups), avoiding repeated evaluations of the black-box model. While this does not change the asymptotic complexity, it makes each split evaluation computationally inexpensive and is critical for practical efficiency; in our experiments, this entire step completes in a few seconds.

Step 3 simply requires fitting the regional shape functions, which depends on the underlying fitting approach. Our default setup uses gradient boosting which is computationally efficient.

Overall our method is efficient, typically fitting most tabular datasets within a few seconds, as shown by the runtimes reported in the Appendix C.

4. Empirical Evaluation

The empirical evaluation of CALM includes three synthetic regression datasets and 25 public real-world tabular datasets—10 for classification and 15 for regression. Across all experiments, CALM is applied with its default configuration: Step 1 uses XGBoost as the black-box model. Step 2 uses PDP-based heterogeneity with $d_{\max} = 2$, $\epsilon = 0.2$, and K remains unconstrained. Step 3 uses standard gradient boosting. All predictive results are reported as mean \pm standard deviation over standard 5-fold cross-validation. Full experimental details are in Appendix C.

Implementation details. We used well-known open-source implementations for all baseline models: [scikit-learn](#) (random forests), [XGBoost](#), [tensorflow](#) (neural networks and NAM), [interpretml](#) (EBM, EB²M), [pygam](#) (SPLINE), and official repositories for [NODE-GA²M](#)(Chang et al., 2022) and [GAMI-Net](#)(Yang et al., 2020).

4.1. Synthetic example

We compare CALM against EBM (as the GAM baseline) and EB²M (as the GA²M baseline) on three synthetic datasets. Both EBM and EB²M are used with their default parameters. Evaluation is based on R^2 performance. Each dataset contains 1000 samples with features drawn from $x_i \sim \mathcal{U}(-1, 1)$. Table 1 summarizes the accuracy of each approach.

Table 1. Synthetic examples: R^2 comparison (mean \pm std. dev. over 5-fold CV).

Dataset	GAM	GA ² M	CALM
Case 1	0.737 ± 0.028	0.974 ± 0.011	0.995 ± 0.002
Case 2	0.479 ± 0.052	0.712 ± 0.036	0.949 ± 0.024
Case 3	0.527 ± 0.023	0.961 ± 0.009	0.975 ± 0.006

Case 1. We set $y = x_1^2 + \log(|x_2|) + 2 \sin\left(\frac{\pi}{2}x_3\right) \mathbf{1}_{x_2 \geq 0} + 2 \cos\left(\frac{\pi}{2}x_3\right) \mathbf{1}_{x_2 < 0}$. Since GAM cannot model the $x_2 - x_3$ interaction, it simplifies the $x_3 \rightarrow y$ effect by averaging the sine and cosine modes into one curve (Fig. 3a, top row), resulting in $R^2 = 0.737$. Both GA²M and CALM capture the interaction correctly, achieving near-perfect accuracy (0.974 and 0.995). However, their interpretability differs. GA²M requires three views to interpret x_3 's effect: (i) the main effect averaging the sine and cosine cases, (ii) a near-zero $x_1 - x_3$ heatmap, and (iii) an $x_2 - x_3$ heatmap capturing the sign-dependent interaction (Fig. 3c, top row). In contrast, CALM simplifies the interpretation with two 1D plots and a clear separation of the regimes by conditioning on x_2 's sign (Fig. 3b, top row).

Case 2. We set: $y = x_0^2 + \log(|x_1|) + 2[\sin\left(\frac{\pi}{2}x_2\right) \mathbf{1}_{x_0 \geq 0, x_1 \geq 0} + \cos\left(\frac{\pi}{2}x_2\right) \mathbf{1}_{x_0 \geq 0, x_1 < 0} + \sin(2\pi x_2) \mathbf{1}_{x_0 < 0, x_1 \geq 0} + \cos(2\pi x_2) \mathbf{1}_{x_0 < 0, x_1 < 0}]$. GAM (Fig. 3a, middle row) merges all four modes into a single curve, limiting its accuracy to $R^2 = 0.479$. GA²M (Fig. 3c, middle row) captures partial structure through two 2D interactions ($x_1 - x_3$ and $x_2 - x_3$) but misses the full 3-way interaction, reaching $R^2 = 0.712$. Furthermore, the model's behavior is hard to grasp, as it requires integrating information from three distinct plots: the main effect and two interaction heatmaps. CALM (Fig. 3b, middle row) separates the four regimes into distinct 1D curves, achieving both high accuracy ($R^2 = 0.949$) and clear interpretability.

Case 3. We set $y = x_1^2 + \log(|x_2|) \sin\left(\frac{\pi}{2}x_3\right)$, where the logarithmic effect of x_2 , $\log |x_2|$, is modulated by the sinusoidal term $\sin\left(\frac{\pi}{2}x_3\right)$, resulting in a general interaction structure. GAM (Fig. 3a, bottom row) fails to capture the interaction and instead fits a blurred sinusoidal curve, leading to low accuracy ($R^2 = 0.527$). GA²M (Fig. 3c, bottom

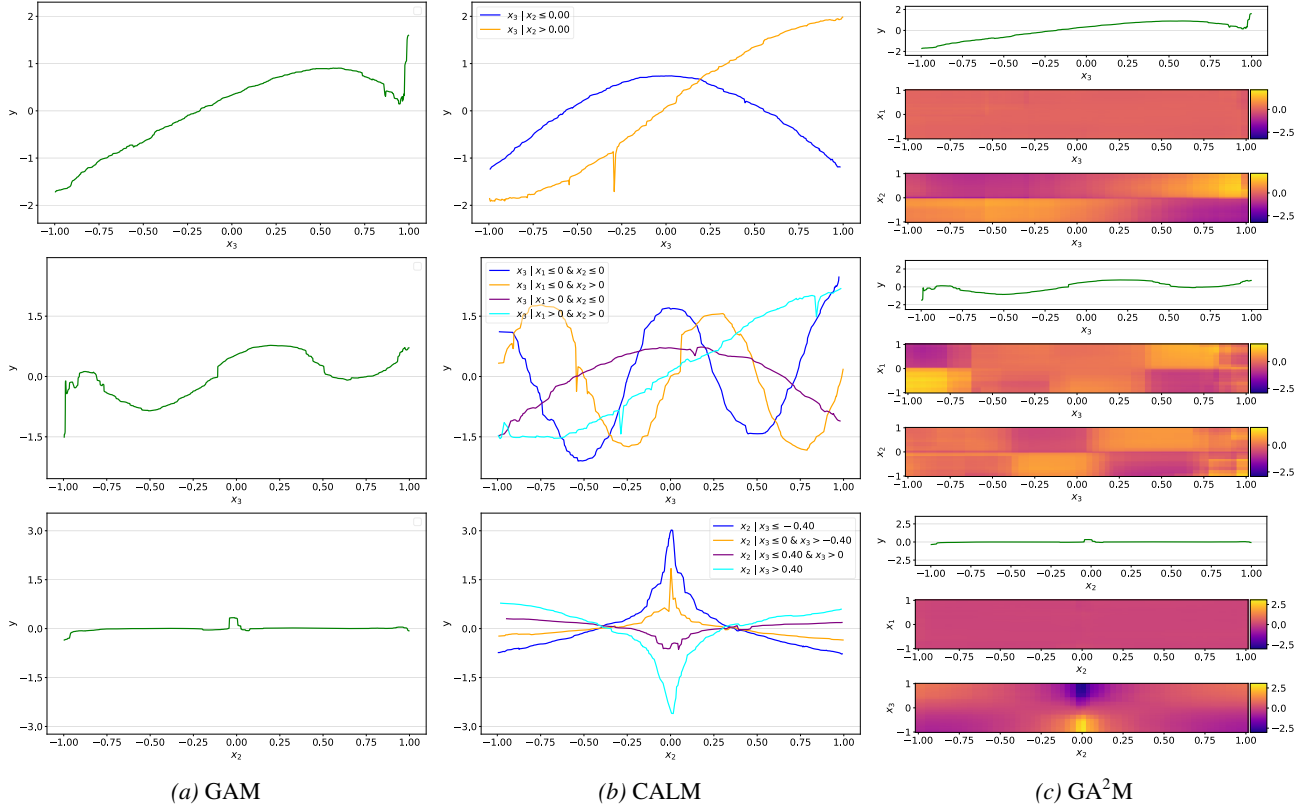


Figure 3. Explanatory plots for the three synthetic regression tasks: top row (Task 1) shows two-region interaction; middle row (Task 2) shows four-region interaction; bottom row (Task 3) shows general interactions.

row) achieves high accuracy ($R^2 = 0.961$) by capturing the interaction in the x_2 - x_3 heatmap. Still, interpretation remains difficult, as understanding the $x_2 \rightarrow y$ effect requires integrating three views: the main effect plot and two interaction heatmaps. CALM (Fig. 3b, bottom row) cannot fully express the continuous x_2 - x_3 interaction, but approximates it by partitioning x_2 and assigning each segment an average logarithmic response. While simplified, this yields a high accuracy ($R^2 = 0.975$) and a concise, transparent explanation that remains *close* to the underlying behavior.

4.2. Evaluation on Real Datasets

On each real dataset, we evaluate CALM against three black-box baselines (neural networks, random forests, and XG-Boost), three GAM models (NAM, EBM, and SPLINE), and three GA²M models: EB²M (EBM with pairwise interactions enabled), NODE-GA²M, and GAMI-Net. Evaluation is based on accuracy for classification tasks and RMSE for regression datasets.

Classification Results. On classification datasets (Table 2), CALM: (i) outperforms the average performance of GAMs in 9/10 datasets and matches it on the remaining one; (ii) outperforms the average performance of GA²Ms on

5/10 datasets and matches it on one case; (iii) outperforms the black-box model on 4/10 datasets of the datasets and matches it on one.

Regression Results. On regression datasets (Table 3), CALM: (i) outperforms the average performance of GAMs in 14/15 datasets and matches it on the remaining one; (ii) outperforms the average performance of GA²Ms on 8/15 datasets and matches it on two; (iii) outperforms the black-box model on 3/10 datasets of the datasets and matches it on two.

Model Complexity. In addition to its strong predictive performance, CALM achieves its results using remarkably few pairwise feature interactions, 6.2 on average for classification and 15.1 for regression. On classification tasks, this is fewer than EB²M (15.2), GAMI-Net (17.6), and NODE-GA²M (97.7). On regression tasks, CALM remains sparser than GAMI-Net (16.3) and NODE-GA²M (87.3), and close to EB²M (14.1), as shown in Tables 6 and 7 of Appendix C. While most GA²M methods allow explicit control over the number of interactions, we apply them using their default configurations. In contrast, CALM does not impose an interaction cap, but still discovers a sparse structure through region-based conditioning.

Table 2. Classification accuracy vs. baselines (mean \pm std. dev. over 5-fold CV). ✓/✗ denotes higher/lower accuracy than the average GAM (or GA^2M) baseline.

Dataset	BB		GAM		CALM		GA^2M		CALM vs.	
	XGB	NAM	EBM			EB ² M	NODE	GAMI	GAM	GA^2M
Adult	0.870 \pm 0.002	0.851 \pm 0.002	0.870 \pm 0.002	0.870 \pm 0.002	0.871 \pm 0.003	0.850 \pm 0.002	0.857 \pm 0.003	✓	✓	✓
COMPAS	0.661 \pm 0.007	0.682 \pm 0.016	0.681 \pm 0.012	0.684 \pm 0.013	0.684 \pm 0.011	0.667 \pm 0.013	0.686 \pm 0.013	✓	✓	✓
HELOC	0.717 \pm 0.013	0.723 \pm 0.011	0.728 \pm 0.014	0.728 \pm 0.012	0.730 \pm 0.012	0.715 \pm 0.008	0.725 \pm 0.012	✓	✓	✓
MIMIC2	0.890 \pm 0.001	0.886 \pm 0.001	0.886 \pm 0.003	0.886 \pm 0.003	0.886 \pm 0.003	0.888 \pm 0.002	0.884 \pm 0.003	✓	✓	✓
Appendicitis	0.868 \pm 0.069	0.848 \pm 0.056	0.877 \pm 0.077	0.878 \pm 0.063	0.869 \pm 0.079	0.849 \pm 0.016	0.764 \pm 0.074	✓	✓	✓
Phoneme	0.898 \pm 0.006	0.808 \pm 0.002	0.821 \pm 0.007	0.861 \pm 0.011	0.863 \pm 0.007	0.869 \pm 0.003	0.876 \pm 0.009	✓	✗	✗
SPECTF	0.862 \pm 0.029	0.839 \pm 0.030	0.894 \pm 0.015	0.894 \pm 0.015	0.882 \pm 0.017	0.820 \pm 0.067	0.874 \pm 0.016	✓	✓	✓
Magic	0.885 \pm 0.004	0.850 \pm 0.006	0.857 \pm 0.005	0.864 \pm 0.004	0.872 \pm 0.003	0.876 \pm 0.004	0.874 \pm 0.003	✓	✗	✗
Bank	0.908 \pm 0.003	0.901 \pm 0.003	0.902 \pm 0.002	0.905 \pm 0.002	0.909 \pm 0.002	0.903 \pm 0.001	0.908 \pm 0.003	✓	✗	✗
Churn	0.958 \pm 0.004	0.885 \pm 0.009	0.886 \pm 0.005	0.946 \pm 0.003	0.957 \pm 0.009	0.954 \pm 0.009	0.952 \pm 0.007	✓	✗	✗

Table 3. Regression RMSE vs. baselines (mean \pm std. dev. over 5-fold CV). ✓/✗ denotes lower/higher RMSE than the average GAM (or GA^2Ms) baseline.

Dataset	BB		GAM		CALM		GA^2M		CALM vs.	
	XGB	NAM	EBM			EB ² M	NODE	GAMI	GAM	GA^2M
Bike Sharing	39.35 \pm 1.38	101.97 \pm 1.31	100.21 \pm 1.01	55.67 \pm 1.22	54.80 \pm 0.96	54.47 \pm 1.58	53.44 \pm 1.90	✓	✗	✗
California Housing	0.45 \pm 0.01	0.61 \pm 0.01	0.55 \pm 0.01	0.51 \pm 0.01	0.49 \pm 0.01	0.50 \pm 0.01	0.51 \pm 0.04	✓	✗	✗
Parkinsons Motor	1.44 \pm 0.09	6.11 \pm 0.16	4.20 \pm 0.09	2.24 \pm 0.13	2.35 \pm 0.06	3.49 \pm 0.31	2.76 \pm 0.31	✓	✓	✓
Parkinsons Total	1.86 \pm 0.08	7.90 \pm 0.10	4.85 \pm 0.11	2.97 \pm 0.09	2.77 \pm 0.06	4.60 \pm 0.53	3.81 \pm 0.66	✓	✓	✓
Seoul Bike	209.6 \pm 3.47	320.2 \pm 4.38	303.7 \pm 3.86	238.9 \pm 1.64	235.2 \pm 1.58	231.0 \pm 4.23	245.82 \pm 8.45	✓	✗	✗
Wine	0.62 \pm 0.01	0.72 \pm 0.01	0.70 \pm 0.01	0.69 \pm 0.02	0.68 \pm 0.01	0.69 \pm 0.01	0.71 \pm 0.00	✓	✗	✗
Energy	67.97 \pm 2.58	89.80 \pm 2.67	85.23 \pm 2.49	83.09 \pm 1.97	77.33 \pm 2.46	82.18 \pm 2.53	180.1 \pm 84.09	✓	✓	✓
CCPP	3.09 \pm 0.09	4.21 \pm 0.05	3.44 \pm 0.08	3.42 \pm 0.07	3.28 \pm 0.07	3.97 \pm 0.07	3.92 \pm 0.07	✓	✓	✓
Electrical	0.04 \pm 0.02	0.04 \pm 0.01	0.02 \pm 0.01	0.02 \pm 0.01	0.02 \pm 0.01	0.01 \pm 0.01	0.02 \pm 0.01	✓	✗	✗
Elevators	0.00 \pm 0.00	0.00 \pm 0.00	0.00 \pm 0.00	0.00 \pm 0.00	0.00 \pm 0.00	0.00 \pm 0.00	0.00 \pm 0.00	✓	✓	✓
No2	0.47 \pm 0.03	0.50 \pm 0.02	0.49 \pm 0.03	0.49 \pm 0.04	0.47 \pm 0.03	0.52 \pm 0.02	0.50 \pm 0.03	✓	✓	✓
Sensory	0.51 \pm 0.03	0.48 \pm 0.01	0.48 \pm 0.01	0.45 \pm 0.02	0.45 \pm 0.02	0.49 \pm 0.01	0.46 \pm 0.03	✓	✓	✓
Airfoil	1.54 \pm 0.10	4.80 \pm 0.20	4.57 \pm 0.15	2.50 \pm 0.15	2.17 \pm 0.09	2.13 \pm 0.11	4.79 \pm 0.21	✓	✓	✓
Skill Craft	0.94 \pm 0.02	0.93 \pm 0.03	0.90 \pm 0.02	0.90 \pm 0.02	0.90 \pm 0.03	0.91 \pm 0.02	1.38 \pm 0.80	✓	✓	✓
Ailerons	0.00 \pm 0.00	0.00 \pm 0.00	0.00 \pm 0.00	0.00 \pm 0.00	0.00 \pm 0.00	0.00 \pm 0.00	0.00 \pm 0.00	✓	✓	✓

Runtime. On classification tasks, CALM is slightly slower than EBM and EB²M, but noticeably faster than the other two GA^2M models (GAMI-Net and NODE- GA^2M), and even faster than NAM, despite the fact that NAM does not model interactions. In regression tasks, CALM exhibits a runtime similar to NAM and EB²M, and remains significantly faster than the remaining GA^2M baselines. Average runtimes across datasets are reported in Tables 8 and 9 (Appendix C).

Summary. Across both classification and regression tasks, CALM consistently outperforms the average GAM models and achieves comparable performance to GAM models in most cases. Remarkably, it surpasses the best individual GA^2M on selected datasets. These gains are achieved with fewer interactions (highlighting the model’s inherent sparsity) and with practical runtimes, significantly lower than those of complex GA^2M architectures. Together, these results demonstrate that CALM strikes an effective balance between accuracy, simplicity, and efficiency.

5. Conclusions

We introduced CALM, a novel class of interpretable-by-design models that bridge the gap between the interpretability of GAMs and the accuracy of GA^2Ms . CALMs model feature interactions using conditional feature effects, a set of univariate shape functions per feature, conditioned on its interacting features. Extensive evaluation shows that conditional effects are sufficient to preserve, or even exceed, the accuracy of GA^2Ms (which only model bivariate interactions), without resorting to 3D plots or heatmaps.

CALM main limitations is that interpretability may harden as the number of interactions increases. Although each feature is linked to a maximum of $2^{d_{\max}} = 4$ shape functions, extensive cross-feature dependencies can clutter plots with vertical lines, making them harder to read. Furthermore, the method’s accuracy is strictly tied to the quality of the underlying black-box and additive models; if either underperforms, the entire predictive output suffers.

References

- Agarwal, R., Melnick, L., Frosst, N., Zhang, X., Lengerich, B., Caruana, R., and Hinton, G. E. Neural additive models: Interpretable machine learning with neural nets. In *Advances in Neural Information Processing Systems*, volume 34, pp. 4699–4711, 2021.
- Angelino, E., Larus-Stone, N., Alabi, D., Seltzer, M., and Rudin, C. Learning certifiably optimal rule lists for categorical data, 2018.
- Bien, J. and Tibshirani, R. Prototype selection for interpretable classification. *The Annals of Applied Statistics*, 5(4), 2011. ISSN 1932-6157. doi: 10.1214/11-aos495.
- Breiman, L., Friedman, J., Olshen, R., and Stone, C. *Classification and Regression Trees*. Chapman and Hall/CRC, 1984. doi: <https://doi.org/10.1201/9781315139470>.
- Candanedo, L. M. Appliances energy prediction dataset, 2017.
- Candanedo, L. M., Feldheim, V., and Deramaix, D. Data driven prediction models of energy use of appliances in a low-energy house. *Energy and Buildings*, 140:81–97, 2017. doi: 10.1016/j.enbuild.2017.01.083.
- Caruana, R., Lou, Y., Gehrke, J., Koch, P., Sturm, M., and Elhadad, N. Intelligible models for healthcare: Predicting pneumonia risk and hospital 30-day readmission. In *Proceedings of the 21th ACM SIGKDD international conference on knowledge discovery and data mining*, pp. 1721–1730, 2015.
- Chang, C.-H., Caruana, R., and Goldenberg, A. Nodegam: Neural generalized additive model for interpretable deep learning. In *International Conference on Learning Representations*, 2022.
- Chen, C., Li, O., Tao, C., Barnett, A. J., Su, J., and Rudin, C. This looks like that: Deep learning for interpretable image recognition. In *NeurIPS*, 2019.
- Doshi-Velez, F. and Kim, B. Towards a rigorous science of interpretable machine learning. *arXiv preprint arXiv:1702.08608*, 2017.
- Friedman, J. H. Greedy function approximation: A gradient boosting machine. *Annals of Statistics*, 29(5):1189–1232, 2001.
- Gkolemis, V., Dalamagas, T., and Diou, C. Dale: Differential accumulated local effects for efficient and accurate global explanations. In *Asian Conference on Machine Learning*, pp. 375–390. PMLR, 2023a.
- Gkolemis, V., Dalamagas, T., Ntoutsi, E., and Diou, C. Rhale: robust and heterogeneity-aware accumulated local effects. In *ECAI 2023*, pp. 859–866. IOS Press, 2023b.
- Gkolemis, V., Tzerefos, A., Dalamagas, T., Ntoutsi, E., and Diou, C. Regionally additive models: Explainable-by-design models minimizing feature interactions. In *Joint European Conference on Machine Learning and Knowledge Discovery in Databases*, pp. 433–447. Springer, 2023c.
- Guidotti, R., Monreale, A., Ruggieri, S., Turini, F., Giannotti, F., and Pedreschi, D. A survey of methods for explaining black box models. *ACM Computing Surveys*, 51(5):1–42, 2018.
- Hastie, T. and Tibshirani, R. *Generalized Additive Models*. Chapman and Hall/CRC, 1990.
- Herbinger, J., Bischl, B., and Casalicchio, G. Repid: Regional effect plots with implicit interaction detection. In Camps-Valls, G., Ruiz, F. J. R., and Valera, I. (eds.), *Proceedings of The 25th International Conference on Artificial Intelligence and Statistics*, volume 151 of *Proceedings of Machine Learning Research*, pp. 10209–10233. PMLR, March 2022.
- Herbinger, J., Dandl, S., Ewald, F. K., Loibl, S., and Casalicchio, G. Leveraging model-based trees as interpretable surrogate models for model distillation. In *European Conference on Artificial Intelligence*, pp. 232–249. Springer, 2023.
- Herbinger, J., Wright, M. N., Nagler, T., Bischl, B., and Casalicchio, G. Decomposing global feature effects based on feature interactions. *Journal of Machine Learning Research*, 25(381):1–65, 2024.
- Hinton, G., Vinyals, O., and Dean, J. Distilling the knowledge in a neural network. In *NeurIPS Deep Learning and Representation Learning Workshop*, 2015.
- Hollmann, N., Müller, S., Eggensperger, K., and Hutter, F. TabPFN: A transformer that solves small tabular classification problems in a second. *arXiv preprint arXiv:2207.01848*, 2022.
- Hu, L., Chen, J., Nair, V. N., and Sudjianto, A. Surrogate locally-interpretable models with supervised machine learning algorithms. *arXiv preprint arXiv:2007.14528*, 2020.
- Ibrahim, S., Afriat, G., Behdin, K., and Mazumder, R. GRAND-SLAMIN' Interpretable Additive Modeling with Structural Constraints. *Advances in Neural Information Processing Systems*, 36:61158–61186, December 2023.
- Kelly, M., Longjohn, R., and Nottingham, K. The uci machine learning repository, 2025. Accessed: [Insert Date Here].

- Kraus, M., Tschernutter, D., Weinzierl, S., and Zschech, P. Interpretable generalized additive neural networks. *European Journal of Operational Research*, 317(2):303–316, 2024. ISSN 0377-2217. doi: <https://doi.org/10.1016/j.ejor.2023.06.032>.
- Letham, B., Rudin, C., McCormick, T. H., and Madigan, D. Interpretable classifiers using rules and bayesian analysis: Building a better stroke prediction model. *The Annals of Applied Statistics*, 9(3), 2015. ISSN 1932-6157. doi: 10.1214/15-aos848.
- Lipton, Z. C. The mythos of model interpretability: In machine learning, the concept of interpretability is both important and slippery. *Queue*, 16(3):31–57, 2018.
- Lou, Y., Caruana, R., and Gehrke, J. Intelligible models for classification and regression. In *Proceedings of the 18th ACM SIGKDD international conference on Knowledge discovery and data mining*, pp. 150–158, 2012.
- Lou, Y., Caruana, R., Gehrke, J., and Hooker, G. Accurate intelligible models with pairwise interactions. In *Proceedings of the 19th ACM SIGKDD international conference on Knowledge discovery and data mining*, pp. 623–631, 2013.
- Molnar, C. *Interpretable Machine Learning*. 2020.
- Murdoch, W. J., Singh, C., Kumbier, K., Abbasi-Asl, R., and Yu, B. Interpretable machine learning: definitions, methods, and applications. *arXiv preprint arXiv:1901.04592*, 2019.
- Oliabev, A. Home equity line of credit (HELOC), 2018. Accessed: [Insert Date Here].
- Pace, R. K. and Barry, R. Sparse spatial autoregressions. *Statistics and Probability Letters*, 33:291–297, 1997.
- ProPublica. Compas data and analysis for 'machine bias', 2016.
- Radenovic, F., Dubey, A., and Mahajan, D. Neural basis models for interpretability. *Advances in Neural Information Processing Systems*, 35:8414–8426, 2022.
- Ribeiro, M. T., Singh, S., and Guestrin, C. "why should i trust you?": Explaining the predictions of any classifier. In *Proceedings of the 22nd ACM SIGKDD International Conference on Knowledge Discovery and Data Mining*, pp. 1135–1144. ACM, 2016.
- Romano, J. D., Le, T. T., La Cava, W., Gregg, J. T., Goldberg, D. J., Chakraborty, P., Ray, N. L., Himmelstein, D., Fu, W., and Moore, J. H. Pmlb v1.0: an open source dataset collection for benchmarking machine learning methods. *arXiv preprint arXiv:2012.00058v2*, 2021.
- Rudin, C. Stop explaining black box machine learning models for high stakes decisions and use interpretable models instead. *Nature machine intelligence*, 1(5):206–215, 2019.
- Saeed, M., Villarroel, M., Reisner, A. T., Clifford, G., Lehman, L.-W., Moody, G., Heldt, T., Kyaw, T. H., Moody, B., and Mark, R. G. Multiparameter intelligent monitoring in intensive care ii (mimic-ii): A public-access intensive care unit database. *Critical Care Medicine*, 39(5):952–960, 2011. doi: 10.1097/CCM.0b013e31820a92c6.
- Tan, S., Caruana, R., Hooker, G., and Lou, Y. Distill-and-compare: Auditing black-box models using transparent model distillation. In *Proceedings of the 2018 AAAI/ACM Conference on AI, Ethics, and Society*, pp. 303–310, 2018.
- Vanschoren, J., van Rijn, J. N., Bischl, B., and Torgo, L. Openml: Networked science in machine learning. *SIGKDD Explorations*, 15(2):49–60, 2013. doi: 10.1145/2641190.2641198.
- Wood, S. N. *Generalized additive models: an introduction with R*. CRC press, 2017.
- Yang, Z., Zhang, A., and Sudjianto, A. Gami-net: An explainable neural network based on generalized additive models with structured interactions. *arXiv preprint arXiv:2003.07132*, 2020.

A. Conditionally Additive Local Models (CALMs)

In the main paper (Algorithm 1), we summarize the procedure of fitting a Conditionally Additive Local Model (CALM):

$$f_{\text{CALM}}(\mathbf{x}) = g^{-1} \left(\beta_0 + \sum_{i=1}^d f_i^{r_i(\mathbf{x}_{-i})}(x_i) \right),$$

as defined in Eq.(1), to a dataset $\mathcal{D} = \{\mathbf{x}^{(i)}, y^{(i)}\}_{i=1}^N$ in three main steps: (i) fit a high-capacity reference model f_{ref} on \mathcal{D} , (ii) fit a partition tree T_i using an interaction-related heterogeneity measure H_i for each feature $i = 1, \dots, D$, and (iii) estimate region-specific effects $\{f_i^{(r)}\}_{r=1}^{R_i}$ for each feature $i = 1, \dots, D$. We provide additional details for each step below.

A.1. Step 1: Fit a high-capacity reference model f_{ref} on \mathcal{D}

The initial stage involves fitting a high-capacity predictive model, denoted as $f_{\text{ref}} : \mathbb{R}^D \rightarrow \mathbb{R}$ to dataset $\mathcal{D} = \{(\mathbf{x}^{(i)}, y^{(i)})\}_{i=1}^N$. The reference model serves as an accurate functional approximation of the underlying relationship between the input features \mathbf{x} and the response variable y . The choice of f_{ref} is flexible; any sufficiently expressive and accurate model can be employed. Commonly used options include gradient-boosted decision trees (e.g., XGBoost, which we adopt by default), deep neural networks, random forests, or more recent architectures such as TabPFN (Hollmann et al., 2022).

A.2. Step 2: Fit a partition tree T_i using heterogeneity H_i for each feature

We first define a suitable heterogeneity measure H_i (see Section A.2.1), and then explore the relationship between heterogeneity and CALM's error in approximating f_{ref} . Motivated by these results, we fit a partition tree T_i for each feature i (see Section A.2.4). Finally, if the user specifies a constraint K on the maximum number of interactions, we apply a pruning step to retain the K most significant interactions (see Section A.2.5).

A.2.1. HETEROGENEITY MEASURES H_i

Interaction-related heterogeneity H_i quantifies the extent to which a feature x_i interacts with all other features x_j , where $j \in \{1, \dots, d\} \setminus \{i\}$. The computation of H_i is based on the variance of local effects: $h(x_i, \mathbf{x}_{-i}^{(j)})$.

Local Effect. We define $h(x_i, \mathbf{x}_{-i}^{(j)})$ as the local effect of feature x_i when applied to the j -th background observation $\mathbf{x}_{-i}^{(j)}$. That is, if we take the j -th observation and substitute the i -th feature with the value x_i , the resulting change (local effect) in the model output is captured by $h(x_i, \mathbf{x}_{-i}^{(j)})$. The computation of $h(\cdot)$ relies on two components: (i) a reference teacher model f_{ref} and (ii) a background dataset $\{\mathbf{x}^{(i)}\}_{i=1}^N$ containing input features only. The specific form of $h(\cdot)$ depends on the chosen feature effect method. Several methods can be used, including Partial Dependence Plot (PDP), SHAP-Dependence Plot (SHAP-DP) and Robust and Heterogeneity-aware ALE (RHALE).

Below, we provide the definition of h in the case of PDP, which we adopt as the default method in our experiments. Let f_{ref} be the reference model and $\{\mathbf{x}^{(j)}\}_{j=1}^N$ the background dataset. The PDP-based heterogeneity is defined as:

$$h(x_i, \mathbf{x}_{-i}^{(j)}) = f_{\text{ref}}(x_i, \mathbf{x}_{-i}^{(j)}) - c(\mathbf{x}_{-i}) \quad (6)$$

where $c(\mathbf{x}_{-i}^{(j)}) = \mathbb{E}_{X_i} [f_{\text{ref}}(X_i, \mathbf{x}_{-i}^{(j)})]$ is a centering constant. For details on alternative approaches, we refer the reader to (Herbinger et al., 2024; 2022).

Point-wise heterogeneity $H_i(x_i)$ and Heterogeneity H_i . The pointwise heterogeneity is then defined as

$$H_i(x_i) = \mathbb{E}_{\mathbf{X}_{-i}} [(h(x_i, \mathbf{X}_{-i}) - \mu_i(x_i))^2] \quad (7)$$

where $\mu_i(x_i) = \mathbb{E}_{\mathbf{X}_{-i}} [h(x_i, \mathbf{X}_{-i})]$ is the mean local effect. Inside a region, this heterogeneity takes the form of Eq. (4). Feature-level heterogeneity is

$$H_i = \mathbb{E}_{X_i} [H_i(X_i)] = \mathbb{E}_{X_i} [\text{Var}_{\mathbf{X}_{-i}} [h(X_i, \mathbf{X}_{-i})]] \quad (8)$$

Inside a region this definition takes the form of Eq. (5).

A more formal motivation for the use of heterogeneity in CALM comes from the proposition of the following section.

A.2.2. HETEROGENEITY AND CALM APPROXIMATION ERROR

Proposition A.1. Let $\mathcal{E} = \mathbb{E}_{\mathbf{X}} \left[(f_{\text{ref}}(\mathbf{X}) - f_{\text{CALM}}(\mathbf{X}))^2 \right]$ be the mean squared error of the CALM approximation of f_{ref} . Assume that $f_{\text{ref}} : \mathcal{X} \rightarrow \mathbb{R}$ admits a multivariate regionally additive approximation

$$f_{\text{ref}}(\mathbf{x}) \approx \beta_0 + \sum_{i=1}^d h_i^{r_i(\mathbf{x}_{-i})}(\mathbf{x})$$

such that each $h_i^{r_i(\mathbf{x}_{-i})}$ captures the contribution of the i -th feature to the function's output (including interactions). Also, assume that there is no error in fitting of the univariate CALM shape functions. Then,

$$\min_{f_{\text{CALM}}} \mathcal{E} \leq d \sum_{i=1}^d \left(\sum_{r=1}^{R_i} P_{\mathcal{R}_i^{(r)}} H_i^{\mathcal{R}_i^{(r)}} \right) \quad (9)$$

where region $\mathcal{R}_i^{(r)}$ is the r -th region of the i -th feature, $P_{\mathcal{R}_i^{(r)}}$ is the probability mass of the region in the data and $H_i^{\mathcal{R}_i^{(r)}}$ is the heterogeneity of $h_i^{\mathcal{R}_i^{(r)}}(\mathbf{x})$.

Proof. For the approximation error we have

$$\begin{aligned} \mathcal{E} &= \mathbb{E}_{\mathbf{X}} \left[(f_{\text{ref}}(\mathbf{X}) - f_{\text{CALM}}(\mathbf{X}))^2 \right] = \mathbb{E}_{\mathbf{X}} \left[\left(\left(\beta_0 + \sum_{i=1}^d h_i^{r_i(\mathbf{x}_{-i})}(\mathbf{x}) \right) - \left(\beta_0 + \sum_{i=1}^d f_i^{r_i(\mathbf{x}_{-i})}(x_i) \right) \right)^2 \right] \\ &= \mathbb{E}_{\mathbf{X}} \left[\left(\sum_{i=1}^d \left(h_i^{r_i(\mathbf{x}_{-i})}(\mathbf{x}) - f_i^{r_i(\mathbf{x}_{-i})}(x_i) \right) \right)^2 \right] \leq d \sum_{i=1}^d \mathbb{E}_{\mathbf{X}} \left[\left(h_i^{r_i(\mathbf{x}_{-i})}(\mathbf{x}) - f_i^{r_i(\mathbf{x}_{-i})}(x_i) \right)^2 \right] \end{aligned}$$

where the last step results from the Jensen's inequality. We therefore have

$$\mathcal{E} \leq d \sum_{i=1}^d \mathcal{E}_i^{r_i(\mathbf{x}_{-i})} \quad (10)$$

Next, we show that the minimum error achieved for each region is equal to the heterogeneity of the local effects. For any measurable function $g_i(x_i)$ and region \mathcal{R} , decompose, using $\mu_i^{\mathcal{R}}(x_i) = \mathbb{E}_{\mathbf{X}_{-i} | \mathbf{X}_{-i} \in \mathcal{R}} [h_i^{\mathcal{R}}(x_i, \mathbf{X}_{-i})]$:

$$h_i(X_i, \mathbf{X}_{-i}) - g_i(X_i) = (h_i(X_i, \mathbf{X}_{-i}) - \mu_i^{\mathcal{R}}(X_i)) + (\mu_i^{\mathcal{R}}(X_i) - g_i(X_i))$$

Taking expectations inside \mathcal{R} and squaring:

$$\begin{aligned} &\mathbb{E}_{X_i, \mathbf{X}_{-i} | \mathbf{X}_{-i} \in \mathcal{R}} \left[(h_i^{\mathcal{R}}(X_i, \mathbf{X}_{-i}) - g_i(X_i))^2 \right] \\ &= \mathbb{E}_{X_i, \mathbf{X}_{-i} | \mathbf{X}_{-i} \in \mathcal{R}} \left[(h_i^{\mathcal{R}}(X_i, \mathbf{X}_{-i}) - \mu_i^{\mathcal{R}}(X_i))^2 \right] \\ &\quad + \mathbb{E}_{X_i} \left[(\mu_i^{\mathcal{R}}(X_i) - g_i(X_i))^2 \right] \\ &\quad + 2\mathbb{E}_{X_i} \left[\mathbb{E}_{\mathbf{X}_{-i} | \mathbf{X}_{-i} \in \mathcal{R}} [h_i^{\mathcal{R}}(X_i, \mathbf{X}_{-i}) - \mu_i^{\mathcal{R}}(X_i)] (\mu_i^{\mathcal{R}}(X_i) - g_i(X_i)) \right] \end{aligned}$$

The cross-term equals zero because:

$$\mathbb{E}_{\mathbf{X}_{-i} | \mathbf{X}_{-i} \in \mathcal{R}} [h_i^{\mathcal{R}}(x_i, \mathbf{X}_{-i}) - \mu_i^{\mathcal{R}}(x_i)] = \mu_i^{\mathcal{R}}(x_i) - \mu_i^{\mathcal{R}}(x_i) = 0$$

by definition of $\mu_i^{\mathcal{R}}$. Therefore:

$$\mathbb{E}_{X_i, \mathbf{X}_{-i} | \mathbf{X}_{-i} \in \mathcal{R}} \left[(h_i^{\mathcal{R}}(X_i, \mathbf{X}_{-i}) - g_i(X_i))^2 \right] = \mathcal{E}_i^{\mathcal{R}} + \mathbb{E}_{X_i} \left[(\mu_i^{\mathcal{R}}(X_i) - g_i(X_i))^2 \right] \geq \mathcal{E}_i^{\mathcal{R}}$$

with equality if and only if $g_i = \mu_i^{\mathcal{R}}$ almost surely. This indicates that within each region, $\mu_i^{\mathcal{R}}$ minimizes the approximation error.

Moreover, from the definition of pointwise heterogeneity:

$$H_i^{\mathcal{R}}(x_i) := \mathbb{E}_{\mathbf{X}_{-i} | \mathbf{X}_{-i} \in \mathcal{R}} \left[(h^{\mathcal{R}}(x_i, \mathbf{X}_{-i}) - \mu_i^{\mathcal{R}}(x_i))^2 \right]$$

Taking the expectation over X_i :

$$H_i^{\mathcal{R}} = \mathbb{E}_{X_i} [H_i^{\mathcal{R}}(X_i)] = \mathbb{E}_{X_i} \left[\mathbb{E}_{\mathbf{X}_{-i} | \mathbf{X}_{-i} \in \mathcal{R}} \left[(h^{\mathcal{R}}(X_i, \mathbf{X}_{-i}) - \mu_i^{\mathcal{R}}(X_i))^2 \right] \right]$$

which gives

$$H_i^{\mathcal{R}} = \mathbb{E}_{X_i, \mathbf{X}_{-i} | \mathbf{X}_{-i} \in \mathcal{R}} \left[(h^{\mathcal{R}}(X_i, \mathbf{X}_{-i}) - \mu_i^{\mathcal{R}}(X_i))^2 \right] = \min \mathcal{E}_i^{\mathcal{R}}$$

i.e., heterogeneity is the minimum approximation error.

Since heterogeneity minimizes the error for each region we can estimate the feature-level error across regions as

$$\min \mathcal{E}_i = \sum_{r=1}^{R_i} P_{\mathcal{R}_i^{(r)}} H_i^{\mathcal{R}_i^{(r)}}$$

where $P_{\mathcal{R}_i^{(r)}}$ is the probability mass of region $\mathcal{R}_i^{(r)}$.

Using this result with Eq. (10), we have

$$\min_{f_{\text{CALM}}} \mathcal{E} \leq d \sum_{i=1}^d \left(\sum_{r=1}^{R_i} P_{\mathcal{R}_i^{(r)}} H_i^{\mathcal{R}_i^{(r)}} \right)$$

□

This result links heterogeneity with the estimation error of the local effect inside a region and motivates the CALM approach for region splitting. The initial assumption about the additive approximation of f_{ref} is a common approach followed by feature effect methods (where the effect of each feature is computed independently). Moreover, the selected local effect function and heterogeneity are solely used for identifying the splitting regions and not as estimators of f_{ref} . Using this result, and especially Eq. (9), the following two sections present the CALM approach for using heterogeneity to define a partition for each feature.

A.2.3. HETEROGENEITY ESTIMATION

For heterogeneity estimation, denote with $\mathcal{I} \subseteq \{1, \dots, N\}$ the index set of active background instances considered in the heterogeneity calculation i.e., those that reside in region $\mathcal{R}_i^{(r_i(\mathbf{x}_{-i}))}$ of the i -th instance. Then, the point-wise heterogeneity at feature value x_i over \mathcal{I} can be estimated by

$$\hat{H}_i^{\mathcal{I}}(x_i) = \frac{1}{|\mathcal{I}|} \sum_{j \in \mathcal{I}} \left(h(x_i, \mathbf{x}_{-i}^{(j)}) - \mu(x_i) \right)^2, \text{ where } \mu(x_i) = \frac{1}{|\mathcal{I}|} \sum_{j \in \mathcal{I}} h(x_i, \mathbf{x}_{-i}^{(j)}) \quad (11)$$

Eq.(11) quantifies the strength of the interactions of the i -th feature, at position x_i , as the variance of the local effects at x_i . To obtain a global measure of these interactions, we average the pointwise heterogeneity over a grid of M values $\{\tilde{x}_i^{(m)}\}_{m=1}^M$ sampled from the domain of x_i :

$$\hat{H}_i^{\mathcal{I}} = \frac{1}{M} \sum_{m=1}^M \hat{H}_i^{\mathcal{I}}(\tilde{x}_i^{(m)}). \quad (12)$$

Algorithm 2 Fitting a Partition Tree T_i for Feature x_i

```

1: Input:  $f_{\text{ref}}$ ,  $\mathcal{D} = \{(\mathbf{x}^{(k)}, y^{(k)})\}_{k=1}^N$ ; Parameters: max depth  $d_{\max}$ , threshold  $\epsilon$ , grid size  $M = 20$ 
2: Output: Binary tree  $T_i$ 
3:
4: function BUILDTREE(node  $\nu$ , depth  $\ell$ , active indices  $\mathcal{I}$ )
5: if  $\ell = d_{\max}$  then
6:   return  $\nu$  {Stop splitting}
7: end if
8: Compute  $H_i^{\mathcal{I}}$  using Eq.(12)
9: Initialize:  $\Delta H_{\max} \leftarrow 0$ 
10: for each feature  $j \neq i$  do
11:   Determine candidate thresholds  $\mathcal{T}_j$  {Default: Unique values if  $x_j$  categorical, else  $M$ -grid (default:  $M = 20$ )}
12:   for each  $\tau \in \mathcal{T}_j$  do
13:     if  $x_j$  is numerical then
14:        $\mathcal{I}_L \leftarrow \{k \in \mathcal{I} : x_j^{(k)} \leq \tau\}$ ,  $\mathcal{I}_R \leftarrow \mathcal{I} \setminus \mathcal{I}_L$ 
15:     else { $x_j$  is categorical}
16:        $\mathcal{I}_L \leftarrow \{k \in \mathcal{I} : x_j^{(k)} = \tau\}$ ,  $\mathcal{I}_R \leftarrow \mathcal{I} \setminus \mathcal{I}_L$ 
17:     end if
18:     Compute  $\Delta H_i$  using Eq. (13)
19:     if  $\Delta H_i > \Delta H_{\max}$  then
20:        $\Delta H_{\max} \leftarrow \Delta H_i$ , Store  $(j, \tau)$  as optimal split
21:     end if
22:   end for
23: end for
24: if  $\Delta H_{\max} > \epsilon$  then
25:   Split node  $\nu$  into  $\nu_L, \nu_R$  using optimal  $(j, \tau)$ 
26:    $\nu_L \leftarrow \text{BUILDTREE}(\nu_L, \ell + 1, \mathcal{I}_L)$ 
27:    $\nu_R \leftarrow \text{BUILDTREE}(\nu_R, \ell + 1, \mathcal{I}_R)$ 
28: end if
29: return  $\nu$ 
30: end function

```

A.2.4. COMPUTING THE PARTITION TREE T_i FOR EACH FEATURE.

For each feature x_i , we construct a binary tree T_i of maximum depth d_{\max} . At each internal node of the tree, we evaluate candidate binary splits based on all features x_j for $j \in \{1, \dots, d\} \setminus \{i\}$. For each candidate splitting feature x_j , we consider a fixed number T of candidate threshold values τ . These candidate thresholds are selected as T equally spaced values over the range of x_j in the training data, i.e., $[\min_k x_j^{(k)}, \max_k x_j^{(k)}]$, where $x_j^{(k)}$ denotes the value of feature x_j for the k -th training instance. Alternatively, users may choose to evaluate all unique observed values of x_j , i.e., $\{x_j^{(k)}\}_{k=1}^N$.

To determine the best split at each node, we compute the heterogeneity drop, which quantifies the decrease in interaction-related heterogeneity of the target feature x_i after performing the split. Specifically, for a candidate split, we partition the current set of instances \mathcal{I} into left and right subsets \mathcal{I}_L and \mathcal{I}_R , based on whether the splitting feature x_j falls below or above the threshold τ . The heterogeneity drop is defined as:

$$\Delta H_i = \frac{H_i^{\mathcal{I}} - \left(\frac{|\mathcal{I}_L|}{|\mathcal{I}|} H_i^{\mathcal{I}_L} + \frac{|\mathcal{I}_R|}{|\mathcal{I}|} H_i^{\mathcal{I}_R} \right)}{H_i^{\mathcal{I}}} \quad (13)$$

where $H_i^{\mathcal{I}}$ denotes the interaction-related heterogeneity of feature x_i over the current set of instances \mathcal{I} ; \mathcal{I}_L and \mathcal{I}_R are the subsets of \mathcal{I} resulting from the candidate split; $H_i^{\mathcal{I}_L}$ and $H_i^{\mathcal{I}_R}$ are the heterogeneities of x_i computed on the left and right subsets, respectively; and $|\mathcal{I}_L|/|\mathcal{I}|$ and $|\mathcal{I}_R|/|\mathcal{I}|$ are the proportions of instances in each subset, which serve as weights in the weighted average.

Algorithm 3 Gradient Boosting for GAM

```

1: Initialize  $f_i \leftarrow 0$  for all  $i = 1, \dots, d$ 
2: for  $m = 1$  to  $M$  do
3:   for  $i = 1$  to  $d$  do
4:      $\mathcal{E} \leftarrow \{(x_j^{(i)}, y^{(j)} - f_{\text{GAM}}(\mathbf{x}^{(j)}))\}_{j=1}^N$  {Compute partial residuals}
5:     Learn shaping function  $S : x_i \rightarrow \mathbb{R}$  using  $\mathcal{E}$  {Fit shape function}
6:      $f_i \leftarrow f_i + \eta S$  {Update with learning rate  $\eta$ }
7:   end for
8: end for

```

Algorithm 4 Gradient Boosting for CALM

```

1: Initialize  $f_i^{(r)} \leftarrow 0$  for all  $i = 1, \dots, d$  and  $r = 1, \dots, R_i$ 
2: for  $m = 1$  to  $M$  do
3:   for  $i = 1$  to  $d$  do
4:     for  $r = 1$  to  $R_i$  do
5:        $\mathcal{E} \leftarrow \{(x_i^{(j)}, y^{(j)} - f_{\text{CALM}}(\mathbf{x}^{(j)})) : \mathbf{x}^{(j)} \in \text{Region}_r(T_i)\}$  {Filter by region  $\mathcal{R}_i^{(r)}$ }
6:       Learn shaping function  $S : x_i \rightarrow \mathbb{R}$  using  $\mathcal{E}$ 
7:        $f_i^{(r)} \leftarrow f_i^{(r)} + \eta S$  {Update regional shape function}
8:     end for
9:   end for
10: end for

```

This normalized metric enhances interpretability by allowing users to define a meaningful threshold, ϵ , for split acceptance. For instance, a user may require a candidate split to achieve a minimum heterogeneity reduction of $\epsilon = 0.2$ (representing a 20% drop) to be considered significant. In our experimental setup, we utilize a default threshold of $\epsilon = 0.2$.

The procedure for fitting the tree T_i is given in Algorithm 2.

A.2.5. PRUNE TREES TO KEEP TOP K INTERACTIONS

If the user sets an upper threshold K on the number of interactions, we want to select the K most important splits. Given the trees T_i for $i = 1, \dots, d$, we denote by ΔH_i^ν the heterogeneity reduction associated with node ν in tree T_i . We collect all such splits ΔH_i^ν across all features i and nodes ν , and then sort them in descending order. From this ordered list, we select the top K nodes that correspond to the largest heterogeneity decreases, while ensuring that no child node is retained without its parent node also being included. Based on this selection, we prune each tree T_i by removing nodes outside the retained set, thereby preserving only the most significant interactions.

A.3. Step 3: Estimating the region-specific effects $\{f_i(r)\}_{r=1}^{R_i}$ for each feature.

The original gradient boosting procedure for fitting a standard, global GAM, $f_{\text{GAM}}(\mathbf{x}) = g^{-1}(\beta_0 + \sum_i f_i(x_i))$, follows the round-robin approach of (Friedman, 2001). At each boosting iteration, one univariate shape function f_i is updated by fitting to the current residuals over the entire dataset, thereby greedily reducing the overall loss. The procedure as described by (Lou et al., 2012) is summarized in Algorithm 3.

To fit a CALM: $f_{\text{CALM}}(\mathbf{x}) = g^{-1}\left(\beta_0 + \sum_{i=1}^d f_i^{r_i}(\mathbf{x}^{(i)})\right)$ we customize the standard gradient boosting to accommodate for region-specific effects, i.e., we adapt this scheme so that each shape function $f_i^{(r)}$ is trained only on the subset of instances that lie within its assigned subregion $\mathcal{R}_i^{(r)}$. This preserves the additive, boosting framework while enforcing that each $f_i^{(r)}$ captures only the behavior of x_i within its corresponding region. The procedure is summarized in Algorithm 4.

A.3.1. THEORETICAL ANALYSIS OF STEP 3

This section formalizes the claims made in Step 3 of the main text. We show that, under squared loss and fixed region-selection trees, (i) the population target of Step 3 is an $L_2(P_X)$ -best approximation of the true regression function onto the

CALM function class, and (ii) an idealized exact version of the algorithm converges to the corresponding empirical risk minimizer.

Consider the CALM score function

$$s(\mathbf{x}) = \beta_0 + \sum_{i=1}^d f_i^{(r_i(\mathbf{X}_{-i}))}(x_i), \quad (14)$$

where the region-selection functions $\{r_i\}$ (or equivalently the trees $\{T_i\}$) are treated as fixed. Let

$$m(\mathbf{x}) = \mathbb{E}[Y \mid \mathbf{X} = \mathbf{x}]$$

denote the true regression function. We assume regression with identity link and squared loss, and $\mathbb{E}[Y^2] < \infty$. We restrict attention to scores $s \in L_2(P_{\mathbf{X}})$ (hence $m \in L_2(P_{\mathbf{X}})$).

To ensure identifiability, we impose the centering condition

$$\mathbb{E}\left[f_i^{(r)}(X_i) \mid r_i(\mathbf{X}_{-i}) = r\right] = 0 \quad \text{for all } i, r \text{ with } \mathbb{P}(r_i(\mathbf{X}_{-i}) = r) > 0. \quad (15)$$

This convention assigns all region-wise constants to the intercept β_0 and ensures uniqueness of the decomposition.

Let $\mathcal{H}(\{T_i\})$ denote the class of all CALM score functions of the form (14) satisfying (15), and assume $\mathcal{H}(\{T_i\}) \subset L_2(P_{\mathbf{X}})$ is a nonempty closed convex set.

A.3.2. POPULATION TARGET

Proposition A.2 (Population optimality). *There exists at least one minimizer*

$$s^* \in \arg \min_{s \in \mathcal{H}(\{T_i\})} \mathbb{E}[(Y - s(\mathbf{X}))^2],$$

and it satisfies

$$s^* \in \arg \min_{s \in \mathcal{H}(\{T_i\})} \mathbb{E}[(m(\mathbf{X}) - s(\mathbf{X}))^2].$$

In particular,

$$\mathbb{E}[(Y - s^*(\mathbf{X}))^2] - \mathbb{E}[(Y - m(\mathbf{X}))^2] = \mathbb{E}[(m(\mathbf{X}) - s^*(\mathbf{X}))^2].$$

Proof. For any measurable function s ,

$$Y - s(\mathbf{X}) = (Y - m(\mathbf{X})) + (m(\mathbf{X}) - s(\mathbf{X})).$$

Taking squares and expectations yields

$$\mathbb{E}[(Y - s(\mathbf{X}))^2] = \mathbb{E}[(Y - m(\mathbf{X}))^2] + \mathbb{E}[(m(\mathbf{X}) - s(\mathbf{X}))^2],$$

since $\mathbb{E}[Y - m(\mathbf{X}) \mid \mathbf{X}] = 0$ eliminates the cross-term. The first term does not depend on s , so minimizing prediction error over $\mathcal{H}(\{T_i\})$ is equivalent to minimizing $\mathbb{E}[(m(\mathbf{X}) - s(\mathbf{X}))^2]$. Existence of s^* follows since $\mathcal{H}(\{T_i\}) \subset L_2(P_{\mathbf{X}})$ is nonempty, closed, and convex. Condition (15) ensures uniqueness of the representation $(\beta_0, \{f_i^{(r)}\})$ for any given $s \in \mathcal{H}(\{T_i\})$. \square

Interpretation. Proposition A.2 shows that, with fixed regions, Step 3 computes an $L_2(P_{\mathbf{X}})$ -best approximation of the true regression function m within the CALM function class. Any remaining error is therefore purely due to the structural limitations of the chosen regions and univariate components, not to the optimization procedure.

A.3.3. EMPIRICAL CONVERGENCE OF EXACT STEP 3

Given i.i.d. data $\{(x^{(k)}, y^{(k)})\}_{k=1}^N$, define the empirical risk

$$\widehat{\mathcal{R}}_N(s) = \frac{1}{N} \sum_{k=1}^N (y^{(k)} - s(x^{(k)}))^2.$$

Proposition A.3 (Convergence of exact cyclic regional backfitting). *Assume fixed trees and squared loss. Consider an idealized version of Step 3 that cyclically updates each $f_i^{(r)}$ by exactly minimizing $\widehat{\mathcal{R}}_N$ over that function using only samples with $r_i(\mathbf{x}_{-i}^{(k)}) = r$, followed by empirical centering implemented by shifting the region-wise sample mean from $f_i^{(r)}$ into the intercept β_0 , so that fitted values (and hence $\widehat{\mathcal{R}}_N$) are unchanged. Then $\widehat{\mathcal{R}}_N$ is non-increasing along the iterates, and the procedure converges (in empirical L_2) to a limit $\hat{s} \in \arg \min_{s \in \mathcal{H}(\{T_i\})} \widehat{\mathcal{R}}_N(s)$. Moreover, the fitted-value vector $(\hat{s}(\mathbf{x}^{(1)}), \dots, \hat{s}(\mathbf{x}^{(N)}))$ is unique.*

Proof. With fixed trees, the CALM score is linear in the collection of shape functions $\{f_i^{(r)}\}$ evaluated on the data, and $\widehat{\mathcal{R}}_N$ is a convex quadratic function of these parameters. On the finite sample, $\widehat{\mathcal{R}}_N$ depends on each $f_i^{(r)}$ only through the finite vector $\{f_i^{(r)}(x_i^{(k)}) : r_i(\mathbf{x}_{-i}^{(k)}) = r\}$, so the problem can be viewed as a finite-dimensional least-squares problem. Each regional update solves the exact least-squares problem for one block of parameters while holding the others fixed, and therefore cannot increase $\widehat{\mathcal{R}}_N$. Although regions overlap across features, all updates jointly optimize a single global objective. Standard results for cyclic block coordinate descent on convex quadratics imply convergence to a global minimizer, and the minimizing fitted values are unique by strict convexity of the quadratic loss in the fitted-value vector. The centering condition (15) ensures a unique decomposition into components. \square

Interpretation. This result shows that Step 3 is not a collection of independent local fits. Instead, it performs a coupled optimization of a single additive predictor with region-gated components, analogous to classical backfitting for GAMs. Under exact updates, this procedure is guaranteed to converge to the best CALM fit for the given data and fixed regions.

B. Formal Proofs for Interpretability Properties

This appendix provides formal characterizations and proofs for the interpretability properties discussed in Section 3.3. For each property, we define it precisely and analyze whether it can be answered exactly under GAM, GA²M, and CALM.

Proposition B.1 (Local Feature Contribution). *Let $\hat{y} : \mathbb{R}^d \rightarrow \mathbb{R}$ be a prediction function, and fix an input $\mathbf{x} = (x_1, \dots, x_d) \in \mathbb{R}^d$. For each index $i \in \{1, \dots, d\}$, we define the local contribution $\phi_i(\mathbf{x}) \in \mathbb{R}$ as a function intended to represent the contribution of feature x_i to the output $\hat{y}(\mathbf{x})$. We analyze whether such a decomposition*

$$\hat{y}(\mathbf{x}) = \sum_{i=1}^d \phi_i(\mathbf{x})$$

is uniquely determined by the structure of the model.

(A) In GAM. Assume the model has the additive form

$$\hat{y}(\mathbf{x}) = \sum_{j=1}^d f_j(x_j),$$

with each $f_j : \mathbb{R} \rightarrow \mathbb{R}$. Then for all $i \in \{1, \dots, d\}$,

$$\phi_i(\mathbf{x}) := f_i(x_i)$$

is well-defined, and

$$\hat{y}(\mathbf{x}) = \sum_{i=1}^d \phi_i(\mathbf{x}).$$

(B) In GA²M. Assume the model includes pairwise interactions:

$$\hat{y}(\mathbf{x}) = \sum_{j=1}^d f_j(x_j) + \sum_{j < k} f_{jk}(x_j, x_k),$$

where each $f_j : \mathbb{R} \rightarrow \mathbb{R}$ and $f_{jk} : \mathbb{R}^2 \rightarrow \mathbb{R}$. Then in general, there does not exist a unique additive decomposition

$$\hat{y}(\mathbf{x}) = \sum_{i=1}^d \phi_i(\mathbf{x})$$

with each $\phi_i(\mathbf{x})$ depending only on x_i .

(C) In CALM. Assume the model has the form

$$\hat{y}(\mathbf{x}) = \sum_{j=1}^d f_j^{(r_j(\mathbf{x}_{-j}))}(x_j),$$

where for each j , $r_j : \mathbb{R}^{d-1} \rightarrow \{1, \dots, R_j\}$ is a region selector and $f_j^{(r)} : \mathbb{R} \rightarrow \mathbb{R}$ is a univariate shape function for region r . Here $\mathbf{x}_{-j} := \mathbf{x} \setminus x_j \in \mathbb{R}^{d-1}$.

Then for all $i \in \{1, \dots, d\}$,

$$\phi_i(\mathbf{x}) := f_i^{(r_i(\mathbf{x}_{-i}))}(x_i)$$

is well-defined, and

$$\hat{y}(\mathbf{x}) = \sum_{i=1}^d \phi_i(\mathbf{x}).$$

Proof. We examine each case separately.

(A) In GAM . By direct substitution, the prediction is an additive sum of univariate functions, each depending only on a single feature x_j . Thus the contribution of feature x_i is uniquely defined as $f_i(x_i)$, and the decomposition is exact.

(B) In GA²M. Suppose, for contradiction, that there exists a decomposition

$$\hat{y}(\mathbf{x}) = \sum_{i=1}^d \phi_i(\mathbf{x}),$$

where each $\phi_i : \mathbb{R}^d \rightarrow \mathbb{R}$ represents the contribution of feature x_i and depends only on x_i , i.e., $\phi_i(\mathbf{x}) = \phi_i(x_i)$.

Then each interaction term $f_{jk}(x_j, x_k)$ must be split between ϕ_j and ϕ_k in such a way that the total sum remains correct and additive over individual features. This is only possible if f_{jk} is additively separable, i.e., if there exist functions $g_j, g_k : \mathbb{R} \rightarrow \mathbb{R}$ such that

$$f_{jk}(x_j, x_k) = g_j(x_j) + g_k(x_k).$$

However, the model does not constrain f_{jk} to be separable. In the general case, f_{jk} is non-separable and depends jointly on x_j and x_k .

Therefore, no decomposition $\sum_i \phi_i(x_i)$ can reproduce the prediction $\hat{y}(\mathbf{x})$ using only univariate terms. The contributions $\phi_i(\mathbf{x})$ are not uniquely determined by the model, and must rely on external assumptions or post-hoc attribution methods.

(C) In CALM. For a fixed input \mathbf{x} , each region function $r_j(\mathbf{x}_{-j})$ returns a unique region index in $\{1, \dots, R_j\}$. The corresponding function $f_j^{(r_j(\mathbf{x}_{-j}))}$ is applied to x_j , yielding a scalar. Thus, the contribution of feature x_i is precisely defined as:

$$\phi_i(\mathbf{x}) := f_i^{(r_i(\mathbf{x}_{-i}))}(x_i),$$

and the model prediction is recovered by summing over all features:

$$\hat{y}(\mathbf{x}) = \sum_{i=1}^d f_i^{(r_i(\mathbf{x}_{-i}))}(x_i) = \sum_{i=1}^d \phi_i(\mathbf{x}).$$

□

The second property asks: *How does the prediction change if we perturb a single feature x_i while keeping all others fixed?* The answer differs across GAM , GA²M, and CALM, as shown below.

Proposition B.2 (Regional Feature Sensitivity)). *Let $\hat{y} : \mathbb{R}^d \rightarrow \mathbb{R}$ be a prediction function. Fix an input $\mathbf{x} \in \mathbb{R}^d$, an index $i \in \{1, \dots, d\}$, and a perturbation $\varepsilon > 0$. Define the prediction change under perturbation of x_i as*

$$\Delta\hat{y} := \hat{y}(\mathbf{x} + \varepsilon \mathbf{e}_i) - \hat{y}(\mathbf{x}).$$

We analyze how $\Delta\hat{y}$ can be computed in GAM , GA²M, and CALM.

(A) In GAM . Assume the model has the additive form

$$\hat{y}(\mathbf{x}) = \sum_{j=1}^d f_j(x_j),$$

with each $f_j : \mathbb{R} \rightarrow \mathbb{R}$ univariate. Then

$$\Delta\hat{y} = f_i(x_i + \varepsilon) - f_i(x_i).$$

(B) In GA²M. We show that in GA²M, the change $\Delta\hat{y}$ caused by perturbing x_i depends on the values of all interacting features x_j for $j \neq i$, and thus cannot be computed from x_i alone.

(C) In CALM: We show that the change in prediction $\Delta\hat{y} := \hat{y}(\mathbf{x} + \varepsilon \mathbf{e}_i) - \hat{y}(\mathbf{x})$ is computable from x_i alone if and only if no region transitions are triggered in other features. Otherwise, the change depends on \mathbf{x}_{-i} , and regional sensitivity is not determined solely by x_i .

Proof. **(A) In GAM.** Since all other features remain unchanged, and their contributions are independent of x_i , we have

$$\hat{y}(\mathbf{x} + \varepsilon \mathbf{e}_i) = \sum_{j \neq i} f_j(x_j) + f_i(x_i + \varepsilon),$$

$$\hat{y}(\mathbf{x}) = \sum_{j \neq i} f_j(x_j) + f_i(x_i),$$

and therefore

$$\Delta\hat{y} = f_i(x_i + \varepsilon) - f_i(x_i).$$

(B) In GA²M. Let $\mathcal{J} := \{j \neq i \mid f_{ij}(x_i, x_j) \text{ is present in the model}\}$, i.e., the set of features that interact with x_i . Since only x_i is perturbed, all other features remain unchanged. The only affected terms are the univariate function $f_i(x_i)$, and the interaction terms $f_{ij}(x_i, x_j)$ for each $j \in \mathcal{J}$. All other terms in the model remain constant.

The prediction after perturbation is:

$$\hat{y}(\mathbf{x} + \varepsilon \mathbf{e}_i) = f_i(x_i + \varepsilon) + \sum_{j \in \mathcal{J}} f_j(x_j) + \sum_{j \in \mathcal{J}} f_{ij}(x_i + \varepsilon, x_j) + C,$$

and before perturbation:

$$\hat{y}(\mathbf{x}) = f_i(x_i) + \sum_{j \in \mathcal{J}} f_j(x_j) + \sum_{j \in \mathcal{J}} f_{ij}(x_i, x_j) + C,$$

where $C := \sum_{j < k, j, k \neq i} f_{jk}(x_j, x_k)$ denotes the interaction terms not involving x_i , which are unaffected.

Subtracting, we obtain:

$$\Delta\hat{y} = f_i(x_i + \varepsilon) - f_i(x_i) + \sum_{j \in \mathcal{J}} [f_{ij}(x_i + \varepsilon, x_j) - f_{ij}(x_i, x_j)].$$

Since this expression depends on interacting x_j for $j \neq i$, it cannot be computed from x_i alone.

(C) In CALM. Assume the model has the form

$$\hat{y}(\mathbf{x}) = \sum_{j=1}^d f_j^{(r_j(\mathbf{x}_{-j}))}(x_j),$$

where $r_j : \mathbb{R}^{d-1} \rightarrow \{1, \dots, R_j\}$ assigns a region index to each feature j based on the context $\mathbf{x}_{-j} := \mathbf{x} \setminus x_j$, and $f_j^{(r)} : \mathbb{R} \rightarrow \mathbb{R}$ is the shape function for region r .

Let $\mathbf{x}_{-i} = \mathbf{x} \setminus x_i$, and define the perturbation $x_i \mapsto x_i + \varepsilon$. Then

$$\Delta\hat{y} = f_i^{(r_i(\mathbf{x}_{-i}))}(x_i + \varepsilon) - f_i^{(r_i(\mathbf{x}_{-i}))}(x_i) + \sum_{j \neq i} \left[f_j^{(r_j(\mathbf{x}_{-j}^{+\varepsilon}))}(x_j) - f_j^{(r_j(\mathbf{x}_{-j}))}(x_j) \right],$$

where $\mathbf{x}_{-j}^{+\varepsilon} := \mathbf{x}_{-j}$ with $x_i \mapsto x_i + \varepsilon$ (since $x_i \in \mathbf{x}_{-j}$ for all $j \neq i$).

Case 1: No region transitions in other features. Assume that for all $j \neq i$, we have $r_j(\mathbf{x}_{-j}^{+\varepsilon}) = r_j(\mathbf{x}_{-j})$. Then:

$$\Delta\hat{y} = f_i^{(r_i(\mathbf{x}_{-i}))}(x_i + \varepsilon) - f_i^{(r_i(\mathbf{x}_{-i}))}(x_i).$$

This case is fully interpretable from the function $f_i^{(r)}$ alone.

Case 2: Region transitions occur in other features. If for some $j \neq i$, the region function changes: $r_j(\mathbf{x}_{-j}^{+\varepsilon}) \neq r_j(\mathbf{x}_{-j})$, then the additional terms contribute:

$$\Delta f_j := f_j^{(r_j(\mathbf{x}_{-j}^{+\varepsilon}))}(x_j) - f_j^{(r_j(\mathbf{x}_{-j}))}(x_j).$$

Hence, the total change includes not only the direct shift in f_i , but also discrete region-based changes in other features and the value of $\Delta\hat{y}$ cannot be recovered from x_i alone. \square

The third property asks whether increasing a feature always increases the model's prediction, regardless of the values of other features. In other words, does the model treat the feature as globally monotonic?

Proposition B.3 (Global Feature Monotonicity). *Let $\hat{y} : \mathbb{R}^d \rightarrow \mathbb{R}$ be a prediction function, and fix a feature index $i \in \{1, \dots, d\}$. Define the global monotonicity condition for feature x_i as follows: the model is said to be globally increasing in x_i if for all $\mathbf{x} \in \mathbb{R}^d$ and all $\delta > 0$,*

$$\hat{y}(\mathbf{x} + \delta \mathbf{e}_i) \geq \hat{y}(\mathbf{x}),$$

and strictly increasing if the inequality is strict.

We analyze whether this property can be verified from the structure of the model.

(A) **In GAM.** Assume the model has the form:

$$\hat{y}(\mathbf{x}) = \sum_{j=1}^d f_j(x_j),$$

with each $f_j : \mathbb{R} \rightarrow \mathbb{R}$.

Then the model is globally increasing in x_i if and only if f_i is monotonically increasing.

(B) **In GA²M.** Assume the model has the form:

$$\hat{y}(\mathbf{x}) = \sum_{j=1}^d f_j(x_j) + \sum_{j < k} f_{jk}(x_j, x_k).$$

Then global monotonicity in x_i cannot be determined from f_i alone.

(C) **In CALM.** Assume the model has the form:

$$\hat{y}(\mathbf{x}) = \sum_{j=1}^d f_j^{(r_j(\mathbf{x}_{-j}))}(x_j),$$

where $r_j : \mathbb{R}^{d-1} \rightarrow \{1, \dots, R_j\}$ is a region selector, and $\mathbf{x}_{-j} := \mathbf{x} \setminus x_j$.

Then global monotonicity in x_i holds if the following two conditions are satisfied:

1. For all regions $r \in \{1, \dots, R_i\}$, the function $f_i^{(r)} : \mathbb{R} \rightarrow \mathbb{R}$ is increasing.
2. For all $j \neq i$, and all $x_j \in \mathbb{R}$, the function $x_i \mapsto f_j^{(r_j(\mathbf{x}_{-j}))}(x_j)$ is non-decreasing; i.e., region transitions caused by changing x_i do not decrease f_j 's contribution.

Proof. (A) **In GAM.** Since the model is additive and each term depends only on a single variable, we have:

$$\hat{y}(\mathbf{x} + \delta \mathbf{e}_i) - \hat{y}(\mathbf{x}) = f_i(x_i + \delta) - f_i(x_i).$$

Thus, $\hat{y}(\mathbf{x} + \delta \mathbf{e}_i) \geq \hat{y}(\mathbf{x})$ if and only if f_i is increasing.

(B) **In GA²M.** As in case (A), $f_i(x_i + \delta) - f_i(x_i)$ gives the direct contribution. However, for each $j \neq i$, the term $f_{ij}(x_i, x_j)$ also contributes. The total change is:

$$\hat{y}(\mathbf{x} + \delta \mathbf{e}_i) - \hat{y}(\mathbf{x}) = f_i(x_i + \delta) - f_i(x_i) + \sum_{j \neq i} [f_{ij}(x_i + \delta, x_j) - f_{ij}(x_i, x_j)].$$

The sign of this expression depends on the values of x_j , and therefore cannot be determined from f_i alone. Consequently, verifying global monotonicity in x_i requires knowing the full interaction structure and input values.

(C) In CALM Let $\mathbf{x} \in \mathbb{R}^d$ and $\delta > 0$. Define:

$$\Delta\hat{y} := \hat{y}(\mathbf{x} + \delta\mathbf{e}_i) - \hat{y}(\mathbf{x}).$$

Then:

$$\Delta\hat{y} = f_i^{(r_i(\mathbf{x}_{-i}))}(x_i + \delta) - f_i^{(r_i(\mathbf{x}_{-i}))}(x_i) + \sum_{j \neq i} \left[f_j^{(r_j(\mathbf{x}_{-j}^{+\delta}))}(x_j) - f_j^{(r_j(\mathbf{x}_{-j}))}(x_j) \right],$$

where $\mathbf{x}_{-j}^{+\delta}$ is obtained by replacing $x_i \mapsto x_i + \delta$ in \mathbf{x}_{-j} .

The first term is non-negative if $f_i^{(r)}$ is increasing for all regions r , and the region $r_i(\mathbf{x}_{-i})$ is fixed.

The second term is a sum over changes in other features' contributions due to possible changes in their regions r_j . For the model to be globally increasing in x_i , all such contributions must be non-negative. This requires that increasing x_i does not cause a decrease in the contribution of any other feature x_j , i.e., region transitions must preserve or increase each f_j .

Therefore, global monotonicity in x_i requires both conditions above. Conversely, if both conditions are satisfied, then each term in the sum is non-negative, implying $\Delta\hat{y} \geq 0$.

□

C. Detailed Experiments

C.1. Experimental Setup Details

Reporting convention. As in Section 4, we report mean \pm standard deviation over 5-fold cross-validation.

Table 5. Regression Datasets

Table 4. Classification Datasets			Table 5. Regression Datasets		
Dataset	Size	Attributes	Dataset	Size	Attributes
Adult	45222	13	Bike Sharing	17379	11
COMPAS	6167	9	California Housing	20640	8
HELOC	10459	23	Parkinsons Motor	5875	19
MIMIC2	24508	17	Parkinsons Total	5875	19
Appendicitis	106	7	Seoul Bike	8465	14
Phoneme	5404	5	Wine	6497	11
SPECTF	349	44	Energy	19735	28
Magic	19020	10	CCPP	9568	4
Bank	45211	16	Electrical	10000	13
Churn	5000	19	Elevators	16599	18
			No2	500	7
			Sensory	576	11
			Airfoil	1503	5
			Skill Craft	3338	19
			Ailerons	13750	39

Datasets details. Tables 4 and 5 summarize the 10 classification and 15 regression datasets used in our experiments. These datasets are sourced from various publicly available repositories. The UCI Machine Learning Repository (Kelly et al., 2025) provides datasets including Adult, Magic, Bank, Bike Sharing, Parkinson’s Motor, Parkinson’s Total, Seoul Bike, Wine, CCPP and Skill Craft. OpenML (Vanschoren et al., 2013) offers datasets such as Electrical, Elevators, No2, Sensory, Airfoil, and Ailerons. The Penn Machine Learning Benchmarks (PMLB) (Romano et al., 2021) includes datasets like Appendicitis, Phoneme, SPECTF, and Churn. Additional datasets used in our experiments include California Housing (Pace & Barry, 1997), MIMIC-II (Saeed et al., 2011), COMPAS (ProPublica, 2016), HELOC (Oliabev, 2018), and Energy (Candanedo, 2017; Candanedo et al., 2017).

Data Preprocessing. All input features are standardized using z-score normalization. For regression tasks, the target variable y is also standard scaled. The only exception is the GAMI-Net model, which requires input features to be scaled using min-max normalization. For RMSE, predictions and targets are inverse-transformed to the original scale prior to evaluation.

Model Configurations. Our black box models comprise a fully connected neural network, a random forest and an XGBoost ensemble. The deep network contains two hidden layers with 50 units each; ReLU activations are used for regression whereas a final sigmoid unit closes the classification variant. Training is carried out for 200 epochs with the Adam optimiser (learning rate=0.001), a batch size of 200 and either mean-squared error or binary cross-entropy loss, depending on the task. The random-forest baseline consists of 500 trees grown to a maximum depth of 25 with a minimum of three samples required at each leaf. For boosted trees we employ XGBoost with 300 boosting rounds, a learning rate of 0.1 and the log-loss evaluation metric for classification

For GAM models we consider NAM and EBM without interactions and Spline. The Neural Additive Model (NAM) builds one independent multilayer perceptron per feature; each sub-network has three hidden layers of 100,100 and 10 ReLU units followed by a linear output, and the additive sum is passed through a sigmoid for binary classification. Training uses Adam (learning rate 0.001), for 10 epochs and a mini-batch size of 32. Spline-GAMs are implemented with PyGAM’s LinearGAM or LogisticGAM, allocating a single spline term to every feature while relying on PyGAM’s automatic smoothing. Finally, the Explainable Boosting Machine (EBM) is used without interaction terms by explicitly setting $n.interactions = 0$.

To capture pairwise interactions we experiment with three GA²M variants. EB²M extends the EBM by enabling interactions with a default strength of 0.9; NODE-GA²M activates its interaction mode via the ga2m=1 flag and restricts training to a five-minute time limit to ensure parity with the other models; GAMI-Net is run with the default hyper-parameters.

Table 6. Number of Interactions per Model in Classification Datasets

Dataset	CALM	EB ² M	NodeGA ² M	GAMINet
Adult	4.2±1.4	12.0±0.0	72.6±3.2	20.0±0.0
COMPAS	1.4±1.7	9.0±0.0	36.0±0.0	20.0±0.0
HELOC	1.1±1.6	21.0±0.0	163.8±4.4	20.0±0.0
MIMIC2	11.5±2.1	16.0±0.0	115.0±3.3	20.0±0.0
Appendicitis	4.0±1.7	7.0±0.0	21.0±0.0	6.2±8.1
Phoneme	8.6±1.6	5.0±0.0	10.0±0.0	10.0±0.0
SPECTF	0.0±0.0	40.0±0.0	273.0±14.4	20.0±0.0
Magic	8.5±2.4	9.0±0.0	44.0±0.6	20.0±0.0
Bank	9.2±2.0	15.0±0.0	104.2±3.2	20.0±0.0
Churn	14.0±0.0	18.0±0.0	137.4±2.9	20.0±0.0
Avg.	6.2	15.2	97.7	17.6

For CALM , we configure the heterogeneity drop threshold to 0.2, determining whether a split is considered statistically significant. The region detector, which measures heterogeneity , relies on Partial Dependence Plots (PDP) for RF and XGBoost black-box models, while for DNNs we consider both PDP and RHALE to measure heterogeneity. The detector evaluates 20 candidate split points per feature. The GAM used within regions is an EBM without interactions and the CALM is applied on top of all three black-box models (DNN, RF, XGBoost).

Compatibility. The GAMI-Net baseline depends on a native binary (lib_ebmcore_mac_x64.dylib) compiled for x86_64 architecture. As a result, it is not compatible with Apple Silicon Macs, and running it on such systems will lead to an architecture mismatch error. This issue is limited to this external model and does not affect any of the proposed methods or other baselines. We provide instructions in the README file to guide such users on running all other methods except GAMI-Net.

Computer Resources. All experiments were conducted on an in-house server with cloud infrastructure equipped with an Intel(R) Core(TM) i9-10900X CPU @ 3.70GHz, 128 GB of RAM. No GPU acceleration was utilized during these experiments.

C.2. Number of Interactions

Number of Interactions (Classification). Table 6 reports the number of feature interactions selected or used by each model across classification datasets. CALM consistently uses significantly fewer interactions than GA²M-style baselines, often by a wide margin. In most datasets, CALM activates less than a third of the interactions compared to NodeGA²M, and even fewer than GAMI-Net’s default of 20. The numbers shown for CALM reflect actual detected regions with interaction-specific behavior, confirming that its compact regionalization mechanism results in sparse and interpretable models.

Number of Interactions (Regression). As shown in Table 7, CALM activates fewer feature interactions than other GA²M-based models in regression tasks. While GAMI-Net and EB²M use a fixed or near-fixed interaction set (e.g., 20 by default), and NodeGA²M often selects over 100 interactions, CALM remains sparse across datasets.

C.3. Practical Runtime

We report the total runtime of each method across all datasets in Tables 8 and 9. For CALM, the reported time includes not only the regions detection fitting steps, but also the training time of the underlying black-box model and the GAM component used within regions. While this inclusion gives a complete view of end-to-end cost, it somewhat disadvantages CALM in comparison to other models, whose runtimes reflect only their own training processes. In practice, the black-box or GAM components can be selected to be lightweight and the blackbox model can be reused or pretrained independently, making CALM’s region discovery step lightweight and modular.

Despite this conservative accounting, CALM’s runtime remains competitive. For example, it often trains faster than or

Table 7. Number of Interactions per Model in Regression Datasets

Dataset	CALM	EB ² M	NodeGA ² M	GAMINet
Bike Sharing	19.3±2.7	10.0±0.0	53.6±1.4	20.0±0.0
California Housing	10.7±2.0	8.0±0.0	28.0±0.0	20.0±0.0
Parkinsons Motor	13.8±4.4	18.0±0.0	126.2±1.7	20.0±0.0
Parkinsons Total	14.4±5.8	18.0±0.0	129.2±3.9	20.0±0.0
Seoul Bike	20.4±1.0	13.0±0.0	83.2±0.7	20.0±0.0
Wine	13.9±3.3	10.0±0.0	54.6±0.5	20.0±0.0
Energy	49.2±4.4	26.0±0.0	192.0±4.5	4.0±8.0
CCPP	1.9±2.2	4.0±0.0	6.0±0.0	5.8±0.4
Electrical	0.0±0.0	12.0±0.0	68.6±3.0	12.0±0.0
Elevators	11.7±3.0	17.0±0.0	115.4±2.1	20.0±0.0
No2	12.8±1.9	7.0±0.0	21.0±0.0	20.0±0.0
Sensory	6.9±4.2	10.0±0.0	54.0±0.9	16.0±4.9
Airfoil	9.3±0.5	5.0±0.0	10.0±0.0	10.0±0.0
Skill Craft	0.0±0.0	18.0±0.0	135.6±2.4	16.0±8.0
Ailerons	41.7±2.6	36.0±0.0	232.4±5.1	20.0±0.0
Avg.	15.1	14.1	87.3	16.3

Table 8. Runtime (Seconds) for Classification Datasets

Dataset	BlackBox	GAM		CALM	GA ² M		
		XGB	NAM		EB ² M	NodeGA ² M	GAMINet
Adult	0.2±0.01	38±2	10±1	36±1	13±2	97±9	718±122
COMPAS	0.1±0.004	10±0.1	2±2	2±0.1	1±0.04	51±1	129±5
HELOC	0.2±0.01	31±6	2±2	17±1	2±0.2	57±0.1	249±60
MIMIC2	0.2±0.01	31±0.3	4±3	26±3	5±1	69±9	359±32
Appendicitis	0.1±0.001	5±0.1	2±4	2±0.1	1±0.5	24±0.1	6±5
Phoneme	0.1±0.01	6±1	3±4	3±3	4±1	61±4	166±38
SPECTF	0.1±0.01	32±0.3	3±4	3±3	4±5	25±0.2	180±13
Magic	0.2±0.003	28±18	5±5	17±3	7±4	98±7	489±63
Bank	0.2±0.04	44±1	5±1	42±3	13±1	98±17	994±265
Churn	0.2±0.01	19±3	2±1	10±4	3±2	56±2	257±32
Avg.	0.2	24	4	16	5	64	355

comparably to GA²M methods such as NODE-GA²M and GAMI-Net, which tend to have high computational overhead. On small and medium-sized datasets like COMPAS, HELOC, California Housing, and Wine, CALM runs in under a minute, showing that its interpretability gains come with reasonable computational cost. On larger datasets such as Bank or Ailerons, CALM’s runtime scales moderately but remains practical.

C.4. Performance Metrics for all Experiments

Performance Summary. We evaluated CALM on 25 datasets using three model classes: DNN, XGB, and RF. For each model and dataset, we compare CALM to both its corresponding GAM baseline and the original black-box model.

In comparisons with GAMs, we match the model structure: for example, CALM-NAM is compared directly to NAM, so the performance difference reflects only the benefit of introducing regional modeling. In comparisons with the black-box, we report the accuracy of the *best* CALM-GAM. For XGB and RF, this is selected across multiple GAM types (NAM, EBM, Spline) using a fixed heterogeneity threshold of 0.2. For DNNs, we first identify the best heterogeneity modeling method (PDP or RHALE) for each GAM, and then select the best-performing GAM among all types. While the threshold is fixed in our experiments, we note that alternative thresholds could yield further improvements.

The results cover six tables: Tables 10–12 report performance on regression datasets using DNN, XGB, and RF respectively, while Tables 13–15 report on the same three model classes for classification datasets. Across these settings, CALM

Table 9. Runtime (Seconds) for Regression Datasets

Dataset	BlackBox	GAM		CALM	GA ² M		
	XGB	NAM	EBM		EB ² M	NodeGA ² M	GAMINet
Bike Sharing	0.1±0.01	18±1	2±1	15±1	19±3	187±31	299±33
California Housing	0.2±0.01	15±0.1	4±2	13±1	16±0.5	200±46	677±147
Parkinsons Motor	0.3±0.003	21±6	5±2	17±2	44±4	193±34	536±88
Parkinsons Total	0.3±0.01	18±0.2	5±3	16±2	40±5	227±76	543±79
Seoul Bike	0.2±0.01	15±0.2	3±3	13±3	12±4	127±18	268±53
Wine	0.2±0.01	12±1	2±3	9±3	3±0.4	62±10	187±20
Energy	0.3±0.01	43±0.4	8±3	82±5	97±15	206±57	253±214
CCPP	0.2±0.004	6±0.1	5±4	8±5	14±2	133±18	88±8
Electrical	0.1±0.002	25±20	9±4	11±5	8±3	112±28	279±43
Elevators	0.3±0.1	25±0.4	7±4	35±5	43±8	181±38	773±269
No2	0.1±0.003	5±0.04	2±0.1	2±0.1	2±0.1	26±0.1	78±1
Sensory	0.1±0.001	10±1	4±6	7±5	2±0.4	27±0.5	74±16
Airfoil	0.1±0.001	4±0.03	3±6	5±6	7±1	51±12	76±34
Skill Craft	0.3±0.003	17±0.2	4±6	9±6	1±0.1	44±0.1	141±52
Ailerons	0.3±0.02	53±1	5±7	70±8	3±0.1	126±36	619±134
Avg.	0.2	19	5	21	21	127	326

consistently outperforms the corresponding GAM baseline. It matches or exceeds the performance of its GAM counterpart in 97.8% and 100% of cases for DNNs (Tables 10, 13), 97.8% and 96.7% for XGB (Tables 11, 14), and 95.6% and 96.7% for RF (Tables 12, 15). These results reflect direct, structure-matched comparisons between CALM and GAMs of the same architecture.

When compared to the black-box models, CALM also achieves strong results. The best CALM-GAM variant outperforms the original black-box in 73.3% of DNN regression cases (Table 10), 33.3% for XGB regression (Table 11), and 26.7% for RF regression (Table 12). In classification, it beats the black-box in 90.0% of DNN cases (Table 13), 50.0% for XGB (Table 14), and 60.0% for RF (Table 15).

Overall, CALM outperforms or matches the corresponding GAM in 219 out of 225 cases (97.3%) and surpasses the black-box in 40 out of 75 cases (53.3%). The rare cases where CALM does not improve over the GAM occur in both regression and classification tasks and almost always correspond to scenarios where the GAM itself performs as well as or better than the black-box. These cases suggest that the underlying function is already well captured by global additive effects, leaving little room for further refinement through regional modeling.

Table 10. RMSE Score for Regression Datasets, DNN

Dataset	BlackBox	GAM			CALM - NAM		CALM - EBM		CALM - Spline	
	DNN	NAM	EBM	Spline	PDP	RHALE	PDP	RHALE	PDP	RHALE
Bike Sharing	42.952±1.460	101.968±1.309	100.211±1.010	100.876±0.868	63.034±0.883	64.941±2.566	58.444±1.637	60.966±2.983	59.868±1.564	62.108±2.989
California Housing	0.519±0.017	0.611±0.011	0.554±0.008	0.632±0.009	0.580±0.012	0.591±0.016	0.522±0.010	0.526±0.009	0.593±0.018	0.597±0.006
Parkinsons Motor	3.654±0.162	6.112±0.158	4.204±0.087	6.027±0.070	4.220±0.192	5.303±0.312	2.681±0.105	3.658±0.324	4.149±0.211	5.318±0.430
Parkinsons Total	5.139±0.102	7.897±0.102	4.847±0.107	7.519±0.072	5.456±0.182	6.776±0.381	3.587±0.030	4.319±0.222	5.408±0.365	6.827±0.209
Seoul Bike	244.967±5.081	320.225±4.377	303.685±3.855	302.020±4.701	269.277±6.414	273.241±8.379	249.457±2.407	245.880±5.153	246.855±3.936	243.926±4.433
Wine	0.700±0.015	0.719±0.009	0.703±0.012	0.736±0.039	0.712±0.005	0.711±0.012	0.695±0.011	0.695±0.012	0.729±0.027	0.734±0.035
Energy	77.139±2.916	89.799±2.665	85.225±2.489	86.498±2.384	89.304±2.480	88.600±2.179	84.347±2.358	83.972±2.557	84.929±1.868	83.526±2.653
CCPP	3.916±0.079	4.213±0.050	3.435±0.076	4.144±0.054	4.205±0.067	4.188±0.079	3.427±0.058	3.379±0.083	3.995±0.061	4.006±0.058
Electrical	0.051±0.009	0.040±0.005	0.018±0.011	0.095±0.005	0.040±0.005	0.040±0.005	0.018±0.011	0.012±0.007	0.094±0.005	0.088±0.003
Elevators	0.002±0.000	0.003±0.000	0.002±0.000	0.002±0.000	0.002±0.000	0.002±0.000	0.002±0.000	0.002±0.000	0.002±0.000	0.002±0.000
No2	0.522±0.012	0.503±0.021	0.492±0.034	0.480±0.032	0.507±0.016	0.501±0.025	0.492±0.030	0.498±0.034	0.485±0.028	0.492±0.033
Sensory	0.522±0.022	0.483±0.014	0.477±0.009	0.482±0.012	0.461±0.025	0.449±0.019	0.447±0.021	0.444±0.012	0.453±0.025	0.446±0.020
Airfoil	2.131±0.131	4.801±0.198	4.565±0.148	4.542±0.121	3.275±0.196	3.143±0.150	2.647±0.194	2.449±0.227	2.697±0.161	2.588±0.248
Skill Craft	1.231±0.195	0.925±0.025	0.901±0.021	2.515±3.092	0.923±0.028	0.918±0.023	0.901±0.021	0.905±0.018	1.652±1.323	2.345±2.792
Ailerons	0.0002±0.000	0.0002±0.000	0.0002±0.000	0.0002±0.000	0.0002±0.000	0.0002±0.000	0.0002±0.000	0.0002±0.000	0.001±0.001	

Table 11. RMSE Score for Regression Datasets, XGB

Dataset	BlackBox		GAM			CALM		
	XGB	NAM	EBM	Spline	NAM	EBM	Spline	
Bike Sharing	39.346±1.375	101.968±1.309	100.211±1.010	100.876±0.868	59.732±1.414	55.667±1.220	56.656±1.320	
California Housing	0.454±0.010	0.611±0.011	0.554±0.008	0.632±0.009	0.566±0.010	0.511±0.010	0.594±0.014	
Parkinsons Motor	1.443±0.094	6.112±0.158	4.204±0.087	6.027±0.070	4.574±0.137	2.243±0.126	4.432±0.185	
Parkinsons Total	1.863±0.079	7.897±0.102	4.847±0.107	7.519±0.072	6.109±0.361	2.968±0.089	5.638±0.288	
Seoul Bike	209.587±3.474	320.225±4.377	303.685±3.855	302.020±4.701	270.365±7.049	238.912±1.643	237.705±2.658	
Wine	0.622±0.012	0.719±0.009	0.703±0.012	0.736±0.039	0.703±0.011	0.693±0.016	0.737±0.043	
Energy	67.967±2.579	89.799±2.665	85.225±2.489	86.498±2.384	87.416±2.894	83.088±1.974	82.747±2.421	
CCPP	3.086±0.090	4.213±0.050	3.435±0.076	4.144±0.054	4.171±0.042	3.419±0.066	4.039±0.036	
Electrical	0.037±0.015	0.040±0.005	0.018±0.011	0.095±0.005	0.040±0.005	0.018±0.011	0.095±0.005	
Elevators	0.002±0.000	0.003±0.000	0.002±0.000	0.002±0.000	0.002±0.000	0.002±0.000	0.002±0.000	
No2	0.473±0.026	0.503±0.021	0.492±0.034	0.480±0.032	0.498±0.022	0.492±0.036	0.479±0.031	
Sensory	0.508±0.028	0.483±0.014	0.477±0.009	0.482±0.012	0.462±0.016	0.450±0.020	0.451±0.029	
Airfoil	1.544±0.100	4.801±0.198	4.565±0.148	4.542±0.121	3.146±0.137	2.503±0.147	2.582±0.130	
Skill Craft	0.938±0.019	0.925±0.025	0.901±0.021	2.515±3.092	0.925±0.025	0.901±0.021	2.167±2.261	
Ailerons	0.0002±0.000	0.0002±0.000	0.0002±0.000	0.0002±0.000	0.0002±0.000	0.0002±0.000	0.0002±0.000	

Table 12. RMSE Score for Regression Datasets, RF

Dataset	BlackBox		GAM			CALM		
	RF	NAM	EBM	Spline	NAM	EBM	Spline	
Bike Sharing	43.247±1.037	101.968±1.309	100.211±1.010	100.876±0.868	61.174±1.544	57.158±1.288	57.823±1.393	
California Housing	0.502±0.012	0.611±0.011	0.554±0.008	0.632±0.009	0.570±0.015	0.515±0.012	0.611±0.025	
Parkinsons Motor	1.477±0.155	6.112±0.158	4.204±0.087	6.027±0.070	4.515±0.094	2.230±0.081	4.349±0.061	
Parkinsons Total	1.869±0.243	7.897±0.102	4.847±0.107	7.519±0.072	5.761±0.259	3.044±0.068	5.393±0.162	
Seoul Bike	225.572±3.086	320.225±4.377	303.685±3.855	302.020±4.701	270.514±8.146	243.910±2.580	240.471±4.337	
Wine	0.618±0.012	0.719±0.009	0.703±0.012	0.736±0.039	0.708±0.006	0.691±0.011	0.726±0.036	
Energy	69.406±2.781	89.799±2.665	85.225±2.489	86.498±2.384	88.448±2.607	84.741±2.520	84.690±2.546	
CCPP	3.378±0.078	4.213±0.050	3.435±0.076	4.144±0.054	4.129±0.057	3.422±0.112	4.029±0.052	
Electrical	0.009±0.009	0.040±0.005	0.018±0.011	0.095±0.005	0.040±0.005	0.018±0.011	0.095±0.005	
Elevators	0.003±0.000	0.003±0.000	0.002±0.000	0.002±0.000	0.002±0.000	0.002±0.000	0.002±0.000	
No2	0.466±0.033	0.503±0.021	0.492±0.034	0.480±0.032	0.481±0.023	0.482±0.031	0.484±0.029	
Sensory	0.446±0.007	0.483±0.014	0.477±0.009	0.482±0.012	0.451±0.022	0.439±0.020	0.442±0.025	
Airfoil	2.196±0.170	4.801±0.198	4.565±0.148	4.542±0.121	3.073±0.143	2.533±0.137	2.627±0.108	
Skill Craft	0.916±0.019	0.925±0.025	0.901±0.021	2.515±3.092	0.926±0.037	0.901±0.022	2.320±2.696	
Ailerons	0.0002±0.000	0.0002±0.000	0.0002±0.000	0.0002±0.000	0.0002±0.000	0.0002±0.000	0.0002±0.000	

Table 13. Accuracy Score for Classification Datasets, DNN

Dataset	BlackBox		GAM			CALM - NAM		CALM - EBM		CALM - Spline	
	DNN	NAM	EBM	Spline	PDP	RHALE	PDP	RHALE	PDP	RHALE	
Adult	0.849±0.002	0.851±0.002	0.870±0.002	0.856±0.001	0.853±0.001	0.854±0.003	0.870±0.003	0.871±0.003	0.857±0.003	0.859±0.003	
COMPAS	0.682±0.011	0.682±0.016	0.681±0.012	0.685±0.012	0.682±0.007	0.681±0.014	0.683±0.011	0.679±0.012	0.683±0.015	0.683±0.011	
HELOC	0.721±0.009	0.723±0.011	0.728±0.014	0.726±0.010	0.723±0.011	0.723±0.013	0.727±0.015	0.728±0.014	0.721±0.012	0.726±0.011	
MIMIC2	0.885±0.003	0.886±0.001	0.886±0.003	0.886±0.003	0.887±0.001	0.886±0.001	0.886±0.003	0.886±0.002	0.886±0.003	0.886±0.003	
Appendicitis	0.877±0.072	0.848±0.056	0.877±0.077	0.887±0.064	0.839±0.025	0.848±0.056	0.897±0.055	0.877±0.077	0.887±0.064	0.887±0.064	
Phoneme	0.815±0.009	0.808±0.002	0.821±0.007	0.832±0.006	0.839±0.012	0.834±0.008	0.858±0.010	0.856±0.008	0.855±0.009	0.852±0.006	
SPECTF	0.814±0.016	0.839±0.030	0.894±0.015	0.845±0.040	0.848±0.036	0.882±0.025	0.885±0.021	0.903±0.014	0.848±0.032	0.782±0.036	
Magic	0.870±0.004	0.850±0.006	0.857±0.005	0.855±0.004	0.860±0.007	0.858±0.004	0.862±0.006	0.860±0.006	0.865±0.005	0.860±0.005	
Bank	0.903±0.003	0.901±0.003	0.902±0.002	0.903±0.002	0.902±0.001	0.903±0.005	0.905±0.003	0.904±0.003	0.906±0.003	0.905±0.005	
Churn	0.938±0.005	0.885±0.009	0.886±0.005	0.889±0.005	0.957±0.010	0.949±0.004	0.953±0.006	0.946±0.006	0.959±0.006	0.941±0.007	

Table 14. Accuracy Score for Classification Datasets, XGB

Dataset	GAM				CALM		
	XGB	NAM	EBM	Spline	NAM	EBM	Spline
Adult	0.870±0.002	0.851±0.002	0.870±0.002	0.856±0.001	0.853±0.002	0.870±0.002	0.858±0.001
COMPAS	0.661±0.007	0.682±0.016	0.681±0.012	0.685±0.012	0.686±0.014	0.684±0.013	0.686±0.016
HELOC	0.717±0.013	0.723±0.011	0.728±0.014	0.726±0.010	0.724±0.011	0.728±0.012	0.726±0.011
MIMIC2	0.890±0.001	0.886±0.001	0.886±0.003	0.886±0.003	0.886±0.001	0.886±0.003	0.886±0.003
Appendicitis	0.868±0.069	0.848±0.056	0.877±0.077	0.887±0.064	0.868±0.069	0.878±0.063	0.878±0.063
Phoneme	0.898±0.006	0.808±0.002	0.821±0.007	0.832±0.006	0.843±0.006	0.861±0.011	0.860±0.010
SPECTF	0.862±0.029	0.839±0.030	0.894±0.015	0.845±0.040	0.857±0.043	0.894±0.015	0.845±0.040
Magic	0.885±0.004	0.850±0.006	0.857±0.005	0.855±0.004	0.863±0.007	0.864±0.004	0.868±0.006
Bank	0.908±0.003	0.901±0.003	0.902±0.002	0.903±0.002	0.903±0.002	0.905±0.002	0.907±0.002
Churn	0.958±0.004	0.885±0.009	0.886±0.005	0.889±0.005	0.954±0.007	0.946±0.003	0.953±0.008

Table 15. Accuracy Score for Classification Datasets, RF

Dataset	GAM				CALM		
	RF	NAM	EBM	Spline	NAM	EBM	Spline
Adult	0.843±0.001	0.851±0.002	0.870±0.002	0.856±0.001	0.853±0.002	0.871±0.003	0.859±0.001
COMPAS	0.662±0.016	0.682±0.016	0.681±0.012	0.685±0.012	0.682±0.016	0.683±0.012	0.685±0.012
HELOC	0.724±0.014	0.723±0.011	0.728±0.014	0.726±0.010	0.723±0.014	0.728±0.014	0.726±0.010
MIMIC2	0.888±0.002	0.886±0.001	0.886±0.003	0.886±0.003	0.886±0.002	0.887±0.002	0.886±0.003
Appendicitis	0.859±0.064	0.848±0.056	0.877±0.077	0.887±0.064	0.848±0.056	0.877±0.077	0.887±0.064
Phoneme	0.898±0.005	0.808±0.002	0.821±0.007	0.832±0.006	0.838±0.005	0.859±0.005	0.859±0.009
SPECTF	0.877±0.027	0.839±0.030	0.894±0.015	0.845±0.040	0.848±0.026	0.894±0.018	0.842±0.048
Magic	0.878±0.004	0.850±0.006	0.857±0.005	0.855±0.004	0.861±0.004	0.864±0.004	0.866±0.005
Bank	0.901±0.004	0.901±0.003	0.902±0.002	0.903±0.002	0.905±0.003	0.907±0.002	0.907±0.002
Churn	0.957±0.005	0.885±0.009	0.886±0.005	0.889±0.005	0.952±0.005	0.951±0.007	0.955±0.006